III-4

Surface, Interface and Thin Films

High light

BL5U, 7U

Momentum-Dependent Two-Dimensional Heavy-Fermion Formation in a Monoatomic-Layer Kondo Lattice $YbCu_2$

T. Nakamura[1,2], H. Sugihara[2], Y. Chen[2], K. Tanaka[3] and S. Kimura[1,2,4]

[1]*Graduate School of Frontier Biosciences, Osaka University, Suita 565-0871, Japan*

[2]*Department of Physics, Graduate School of Science, Osaka University, Toyonaka 560-0043, Japan*

[3]*UVSOR Synchrotron Facility, Institute for Molecular Science, Okazaki 444-8585, Japan*

[4]*Department of Materials Molecular Science, Institute for Molecular Science, Okazaki 444-8585, Japan*

Heavy-fermion (HF) systems in rare-earth intermetallic compounds originating from the hybridization between localized *f* electrons and conduction (*c*) electrons are central topics in strongly correlated electron systems [1]. Depending on the *c-f* hybridization strength at low temperatures, the ground state changes from a magnetic order to a heavy Fermi liquid. The competition between these two states makes a quantum critical point, resulting in the emergence of exotic quantum phenomena such as non-Fermi liquid and HF superconductivity [2]. The dimensionality of the system characterizes the fundamental physical property. The combination of the HF state and low dimensionality modifies the ground state because the order parameter of these systems is much more sensitive to dimensionality [3]. However, the monoatomic-layer Kondo-lattice showing a two-dimensional (2D) HF state has never been reported. In this study, we report the HF electronic structure of the monoatomic-layer Kondo lattice $YbCu_2$ by angle-resolved photoelectron spectroscopy (ARPES) at UVSOR-III BL5U and BL7U [4].

Figure 1(a) shows the ARPES intensity plot around the $\bar{\Gamma}$ point at 7 K. The flat band is close to E_F and highly dispersive hole bands are observed near the $\bar{\Gamma}$ point. According to the DFT calculation, the flat band and hole bands originate from the Yb^{2+} $4f_{7/2}$ and the mixing of the Yb 5*d* and Cu *sp* and *d* orbitals [4]. The Yb^{2+} 4*f* flat band is modulated at the cross points to the conduction bands just below E_F, providing evidence of the *c-f* hybridization.

The temperature dependence of the quasiparticle peak just below E_F, the so-called Kondo-resonance (KR) peak, is reflected in renormalization due to the development of *c-f* hybridization. Figure 1(b) shows the angle-integrated (AI) photoelectron spectra as a function of temperature. The KR peak energy is shifted to the E_F with decreasing temperature, indicating the evolution of the renormalization. Figure 1(f) shows the temperature dependence of the KR peak positions. The peak position shifts with decreasing temperature and is saturated at 30 K. Such saturated temperature represents a coherence temperature (T_{coh}), at which the *c-f* hybridization state is fully established, resulting in a HF state [5].

To investigate the momentum-dependent *c-f* hybridization, we took the temperature-dependent peak position of the KR peak at three wavenumbers (k_x = 0.5, 0.0, −0.1 Å^{-1}) as shown in Figs. 1(c-e). The change of the peak position at k_x = 0.5 Å^{-1} almost follows the AI one. In contrast to the saturated feature in the AI spectrum at T = 30 K, the KR peak positions at k_x = 0.0 and −0.1 Å^{-1} are shifted to the higher-binding energy side below T_{coh}, suggesting the hybridization gap enlargement.

[1] P. Coleman *et al.*, J. Phys.: Condens. Matter **13** (2001) R723.
[2] C. Pfleiderer, Rev. Mod. Phys. **81** (2009) 1551.
[3] S. Sachdev, Science **288** (2000) 475.
[4] T. Nakamura *et al.*, Nat. Commun. **14** (2023) 7850.
[5] H. Anzai *et al.*, J. Phys. Soc. Jpn. **91** (2022) 114703.

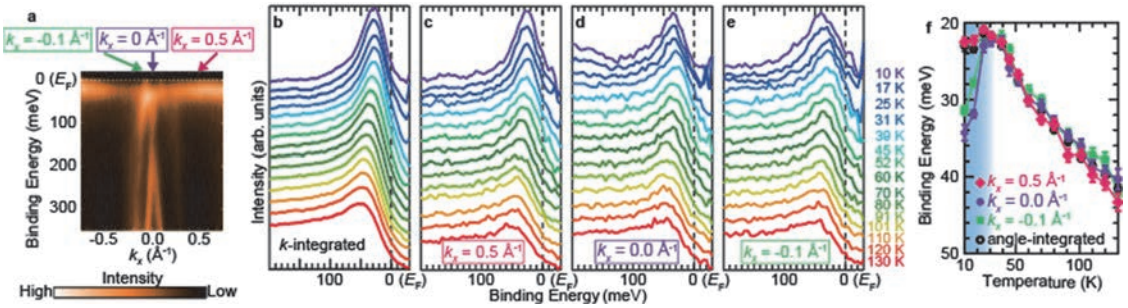

Fig. 1. (a) The ARPES intensity plot around $\bar{\Gamma}$ point taken with horizontally polarized 37-eV photons at 7 K. (b) Angle-integrated photoelectron spectra as a function of temperature taken with horizontally polarized 35-eV photons. The intensity is normalized by the Fermi–Dirac distribution function convolved with the instrumental resolution. (c-e) Angle-resolved photoelectron spectra near E_F as a function of the temperature. The *k*x positions at (c) 0.5, (d) 0.0, and (e) −0.1 Å^{-1} are representative of the local *f* state only, the $\bar{\Gamma}$ point, and the crossing point of the *c-f* hybridization, respectively. (f) Momentum dependence of the energy position of the quasiparticle peak plotted on a linear temperature scale.

BL2A

Surface Treatment Dependence of Mo L-Edge NEXAFS Spectrum of Molybdenum Oxide

E. Kobayashi [1], S. Yoshioka [2] and K. K. Okudaira [3]

[1]*Kyushu Synchrotron Light Research Center, 8-7 Yayoigaoka, Tosu, Saga 841-0005, Japan*

[2]*Graduate School of Engineering, Kyushu University, 744 Motooka Nishi-ku Fukuoka 819-0395 Japan*

[3]*Graduate School of Science and Engineering, Chiba University, 1-33 Yayoi-cho Inage-ku, Chiba 263-8522, Japan*

In recent years, organic thin film solar cells have attracted attention as a new energy source from the perspective of global environmental and energy issues [1, 2]. For the spread of solar cells, it is essential to improve the performance of organic thin film solar cells with low power generation costs, but in recent years, energy conversion efficiency has improved rapidly and is reaching the level of practical use. Solar cells use metal oxide electron and hole transport materials. Further improvement of its performance requires knowledge of the interface between organic molecules and metal oxides [3, 4]. We are investigating surface treatments of metal oxides to improve contact between metal oxide and organic molecules. It is important to find an appropriate surface treatment method because defects on the surface of the oxide film cause charge trapping and reduce conversion efficiency. In this paper, we focused on molybdenum oxide, a typical metal oxide, as a hole transport material.

The sample are molybdenum oxide thin film fabricated on silicon using the RF magnetron sputtering method. The thin film was cleaned with neutral detergent, distilled water, and acetone. One of the films was UV ozone cleaned after its cleaning. NEXAFS spectra of the molybdenum oxide thin film using both total electron yield (TEY) and partial fluorescence yield (PFY) modes were measured at the beamline 2A of the UVSOR in the Institute of Molecular Science. For TEY, the drain current from the sample was measured. For PFY, fluorescence X-rays were collected using an energy dispersible silicon drift detector (SDD). All experiments were performed at room temperature.

Figure 1 shows the NEXAFS spectrum of molybdenum oxide thin film cleaned with neutral detergent, distilled water, acetone, and UV ozone in TEY mode. The overall shape of the spectrum remains unchanged. However, the shape of the main peak changes. Figure 2 is an enlarge view of the spectrum. The peak intensity of the spectrum of the thin film washed with distilled water is higher than that of the untreated one. This indicates that oxidation of the surface layer of the thin film is progressing. In addition, in the spectrum of the thin film after ozone cleaning, the rise of the spectrum shifted to the high energy side, and components on the high energy side appeared. This indicates that the oxidation state on the surface has become a high oxidation state.

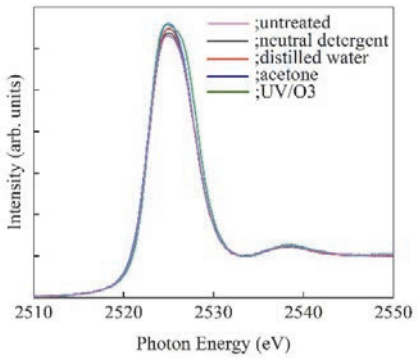

Fig. 1. Mo L-edge NEXAFS spectra of molybdenum oxide thin film in TEY mode.

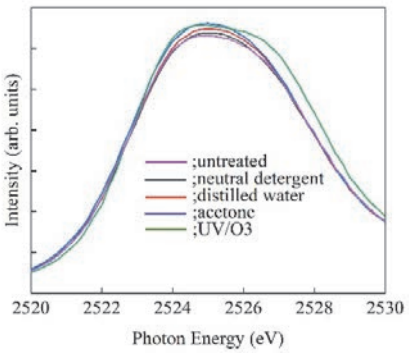

Fig. 2. Enlarged view of Mo L-edge NEXAFS spectra of molybdenum oxide thin film in TEY mode.

[1] Y. Sun *et al*., Adv. Funct. Mater. **31** (2021) 2010000.
[2] L. Ma *et al*., Adv. Mater. **35** (2023) 2208926.
[3] J. Subbigh *et al*., Org. Electron. **11** (2010) 955.
[4] Y. Gong *et al*., J. Mater. Chem. A **8** (2020) 978.

BL2A

Characterization of Electronic Structure in (Ba, Sn)S Thin Film Using XANES

T. Nagai[1,2], H. Murata[3], H. Tampo[1] and F. Kawamura[4]

[1]*Research Institute for Energy Conservation, National Institute of Advanced Industrial Science and Technology (AIST), 1-1-1 Umezono, Tsukuba 305-8568, Japan*

[2]*Graduate School of Science and Engineering, Kagoshima University, 1-21-40 Korimoto 890-0065, Japan*

[3]*Department of Materials Science, Osaka Metropolitan University, Sakai 599-8531, Japan*

[4]*Research Center for Materials Nanoarchitectonics (MANA), National Institute for Materials Science (NIMS), Namiki1-1, Tsukuba 305-0044, Japan.*

SnS(*Pmma*) is one of the great promising semiconductor materials to make the next generation solar cells [1]. Recently, we have shown by first-principles calculations that the bandgap energy of SnS changes with the effective coordination number (ECoN) induced by changes in cell volume [2]. In the real world, however, it is quite difficult to change only the ECoN without changing the volume of the cell, while theoretical calculations make this situation easy to achieve. Therefore, there is no evidence for experimental data for these relationship between the bandgap energy and ECoN at present. Here we noticed that this situation can be achieved by substituting Sn with Ca, Ba, and Sr, elements that have the same valence as Sn divalent and a larger ionic radius than Sn divalent.

According to this idea, the (Ba,Sn)S thin films with the Ba contents {Ba/(Sn+Ba) molar ratios} from 0 to 0.49 were deposited on the soda-lime glass using molecular beam epitaxy (MBE) techniques. Firstly, we measured the X-ray diffraction (XRD) pattern for these films to confirm the impacts of substitution of Sn with Ba to the lattice constant. As a result, the peak position derived from SnS(111) gradually shifts to the lower angle side with increasing Ba content. This experimental result means that the cell volume of SnS becomes larger with increasing of the Ba contents. Moreover, we confirmed that the bandgap energy increased with increasing of Ba contents by the absorption spectra and inverse- and ultraviolet photoemission spectra (IPES and UPS). These experimental results are consistent with our theoretical calculations, showing that the band gap is strongly negatively correlated with the lattice constant, an opposite phenomenon to that of general semiconductors.

Moreover, X-ray absorption near edge structure (XANES) measurements were conducted using BL2A in UVSOR (Okazaki, Japan) to understand the impacts of substitution of Sn with Ba in these films to the electronic structure of SnS. Figure 1 shows the S-K XANES spectra by the partial fluorescence yield method using a silicon drift detector for these (Ba, Sn) S thin films with Ba contents from 0 to 0.49. The white line appeared at 2472 eV for SnS (Ba contents of 0) film. Two additional peaks appeared at 2474 eV and 2479 eV in the (Ba,Sn)S thin film with Ba content above 0.11. Moreover, the white line at 2472 eV for the (Ba,Sn)S films with Ba contents below 0.17 suddenly changed to 2470 eV for the films with Ba contents over 0.27.

Here, previous XRD experiments have confirmed that the signal attributed to SnS disappears at Ba concentrations above 0.15, indicating that a phase transition from a crystalline structure to an amorphous structure is expected to have occurred. Therefore, the energy shifts of the white line from 2472 to 2470 in the S-K XANES of the (Ba,Sn)S thin film containing Ba above 0.27 may reflect a phase transition from a crystalline to an amorphous structure.

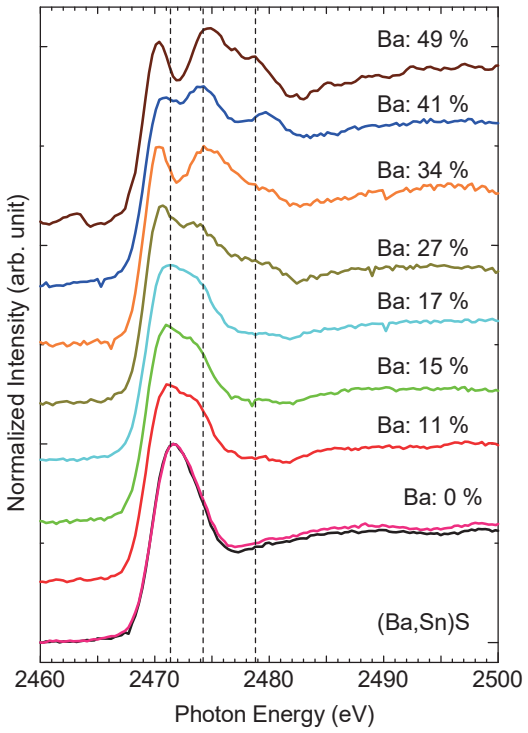

Fig. 1. S-*K* XANES spectra for (Ba, Sn)S thin films with Ba contents from 0 to 0.49.

[1] C. Chotia *et al*., J. Mater. Sci.: Mater. Electron. **32** (2021) 10702.
[2] F. Kawamura *et al*., Sci. Rep. **12** (2022) 7434.

BL3U

X-ray Absorption Spectroscopy Study of Dodenanethiol on Gold Surfaces

F. Sato[1], I. Imahori[1], I. Tsukamoto[1], S. Ohno[1], Y. Sugimoto[2] and M. Nagasaka[2]
[1]*Graduate School of Engineering, Yokohama National University, Yokohamai 240-8501, Japan*
[2]*Institue for Molecular Science, Okazaki 444-8585, Japan*

It is important to understand the behavior of biomolecules on solid surfaces for the application to medical device, biosensor and biocompatible material. It is essential to study the adsorption and desorption behavior of biomolecules and their response to the applied electric fields. It is of particular importance to analyze the dynamic behavior of biomolecules on a surface in electrolyte solutions, which is close to the realistic condition in the body of living creatures [1,2].

In the present study, potential-dependent adsorption and desorption behavior of Dodecanethiol on Au membrane surfaces have been investigated using soft X-ray absorption spectroscopy (XAS) in the transmission mode. The experiments were performed on the soft X-ray undulator beam line at UVSOR-III, BL3U. We used H_2SO_4 and KOH as the electrolyte solution. For the adsorption of Dodecanethiol molecules, the samples were immersed in 100mM Dodecanethiol/ethanol solution for more than 1 hour.

In our previous study [1], we have investigated some biomolecules on Au surfaces using surface differential reflectance spectroscopy (SDRS) and cyclic voltammetry (CV) combined with XAS. The key issue was the interaction between functional group (-COOH) and the applied biases and pH conditions. Redox processes involving charge transfer were clearly observed with CV and the relation between the change in the reflectance spectra and the peaks in CV was investigated in detail. We discovered the indication of the precursor behavior to cause significant change in the reflectance spectra with no corresponding signal in CV. This indicates that such changes in the reflectance spectra are not due to the charge-transfer-type reactions but rather to the subtle change in the orientation/conformation of those biomolecules. Motivated by these works, we here applied XAS to investigate the self-assembled monolayer (SAM) composed of alkanethiol molecules. Here, we selected Dodecanethiol as the representative of this sort of molecules.

To our knowledge, there has been no serious effort to study the Dodecanethiol/Au interfaces using XAS in terms of the aforementioned precursor phenomena. Here, we report the indication of the structural change in the alkanethiol molecule more accurately.

Figure 1 shows the C K-edge XAS spectra obtained for Dodetanethiol adsorbed Au. A distinct peak at 292.5 eV is assigned to the 1s →σ* transition of the C-C bonding [2]. Hence, we could confirm that the detection of the K-edge absorption for the alkanethiol molecules is an effective means to investigate the adsorption behavior of them at the solid/liquid interface.

When the bias of -1.0 eV is applied to the Au substrate for 1 hour, the reduction of the peak intensity was observed. This indicates that the amount of adsorbed Dodecanethiol decreases or some structural changes occur. It should be noted that no peak features are observed within the bias range of -1.0 to 0.0 eV in the CV voltammogram. Therefore, the origin of the spectral change should be due to the quasi-static reaction rather than the reduction reaction.

In the present study, we performed some supplementary CV measurements using potassium ferrocyanide trihydrate ($K_4[Fe(CN)_6]$) to investigate the stability of Dodecanethiol adsorption. We compared with the Dodecylamine for the stability against the applied bias of -1.0 V on the Au substrate. Our preliminary results indicate that the partial removal of Dodecanethiol occurs while all the molecules are removed in the case of Dodecylamine. This suggests that the attachment and removal of the alkanethiol unit can be well-controlled by changing the functional group as well as the condition of the applied bias.

We expect that the present findings would be worthwhile to develop the biodevices utilizing the interaction between the alkanethiol unit ant the Au electrode in general.

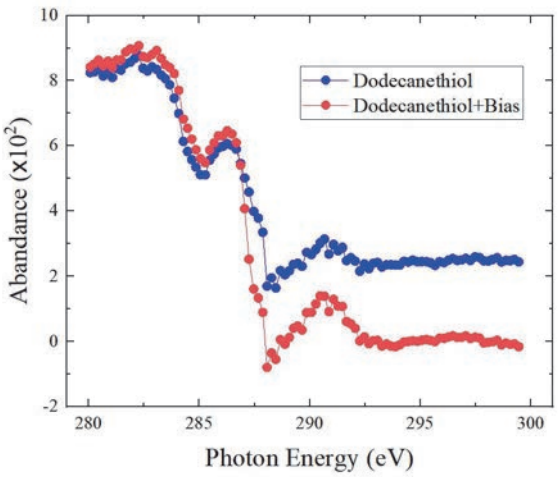

Fig. 1. C K-edge XAS spectra obtained for Dodecanethiol adsorbed Au.

[1] F. Sato *et al.*, UVSOR Activity Report **50** (2023) 145.
[2] A. Imanishi *et al.*, Surf. Sci. **407** (1998) 282.

III-4

BL3U

Ionic Layers at the Electrode Interface of Ionic Liquids Studied Using Interface-Selective Soft X-ray Absorption Spectroscopy

T. Furuya[1], Y. Sugimoto[2], M. Nagasaka[2] and N. Nishi[1]
[1]*Graduate School of Engineering, Kyoto University, Kyoto 615-8510, Japan*
[2]*Institute for Molecular Science, Okazaki 444-8585, Japan*

Ionic liquids (ILs), which are entirely composed of cations and anions, are appealing materials as electrolytes for energy devices. In such devices, the electrochemical interface between ILs and electrodes is an electrochemical reaction field that strongly influences the local reaction rate and thereby the net ones such as charging speed for batteries. Thus, it is of crucial importance to study, and further control, the interfacial structure of ILs at the electrode interface. In the present study, we adopted soft X-ray absorption spectroscopy (XAS) to reveal the interfacial structure of ILs at the electrode interface in an interface-selective manner [1].

An equimolar amount of lithium bis(fluoro-sulfonyl) amide ($Li^+[FSA^-]$) and tetraglyme (G4) were mixed to prepare a solvate IL [2]. *In-situ* XAS measurements for the IL/electrode interface were performed at BL3U at UVSOR-III, by using an electrochemical liquid flow cell [1]. The IL was sandwiched with two Si_3N_4 membranes in the He-filled chamber and XA spectra were measured in transmission mode for the oxygen and fluorine K-edge regions. The photon energy was calibrated by the main peak (530.88 eV) in the oxygen K-edge region for a ProLINE polymer thin film [3]. The thickness of the IL film was controlled with the He pressure in a range from 20 to 2000 nm [4]. For a thick IL film at a low He pressure, the XA spectra can be regarded to originate from the IL bulk with a minor contribution from the interfacial structure, while for a thin IL film at a high He pressure, XA spectra show some features different from the bulk ones, stemming from the interfacial structure. The gold film deposited at the inner surface of one of the two Si_3N_4 membranes was used as the working electrode. Pt wires, as the quasi-reference and counter electrodes, were located aside the film region inside the electrochemical cell. The potential of the working electrode with respect to the quasi-reference electrode was controlled using a potentiostat.

The oxygen K-edge XA spectra for the IL bulk showed a broad absorption peak which is mainly assignable to G4. The double sharp peaks assignable to FSA^- were hardly discernible, hidden in the broad peak. When negative potentials were applied at the IL/gold interface, the interfacial structure started to show the double peak feature, which is likely to be due to the enrichment of FSA^- over G4.

Figure 1 shows the fluorine K-edge XA spectra for the IL bulk and for the IL/gold interface with several applied potentials. The XA spectra showed three potential-dependent features; with lowering the potential, the lowest-energy peak was red-shifted, the second lowest-energy peak was broadened, and the intensity at the high-energy region became higher. Figure 2 shows the redshift, which is large as much as 0.5 eV. These features clearly demonstrate that the present XAS measurements in transmission mode with a nm-scale thin film setup sensitively detect the interfacial structure, which is different from the bulk one and is also potential-dependent.

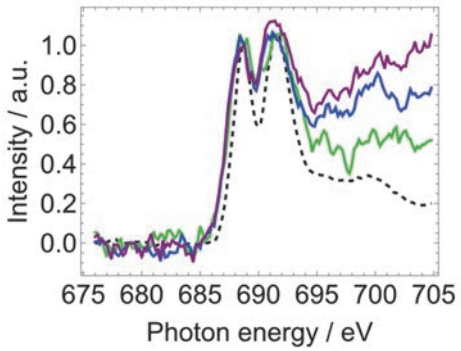

Fig. 1. Fluorine K-edge XA spectra for the IL bulk (black dashed) and for the IL/gold interface at −2 (green), −2.5 (blue), and −3 V (purple), respectively.

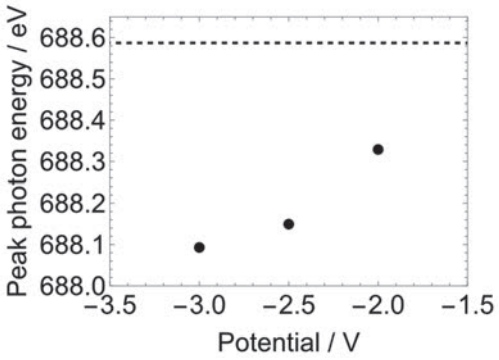

Fig. 2. Peak photon energy as a function of the electrode potential for the lowest energy peak in Fig.1. The horizontal dashed line is for the IL bulk.

[1] M. Nagasaka *et al.*, Rev. Sci. Instrum. **85** (2014) 104105.
[2] S. Terada *et al.*, Aust. J. Chem. **72** (2019) 70.
[3] M. Nagasaka *et al.*, J. Electron Spectrosc. Relat. Phenom. **224** (2018) 93.
[4] M. Nagasaka *et al.*, J. Electron Spectrosc. Relat. Phenom. **117** (2010) 130.

BL3U

Probing Interfacial Water on SiO_2 in Colloidal Dispersion

Y. Hao[1], S. Wang[1], M. Nagasaka[2], Z. Abbas[3] and X. Kong[3]

[1]*Department of Environmental Sciences, College of Urban and Environmental Sciences, Northwest University, Xi'an, China*

[2]*UVSOR Synchrotron, Institute for Molecular Science, Okazaki 444-8585, Japan*

[3]*Department of Chemistry and Molecular Biology, Atmospheric Science, University of Gothenburg, SE-413 90 Gothenburg, Sweden*

Solid surfaces either hard or soft, such as proteins [1], induce significant effect on the structure of water molecules present near the surfaces [2]. Interfacial water is considered to play a role in protein recognition [3] and also has an effect on electrochemical and catalytic reactions at the interfaces [4]. Knowledge about the arrangement of solvent molecules around colloidal nanoparticles is crucial for understanding and evaluation of their reactivity in the water environment as well as their interaction with biological components. In colloidal dispersion such as SiO_2 dispersion in water, the structure of solvent molecules around nanomaterials has not been fully explored. The hydrophilicity, size of nanoparticles and their surface charge affect the interfacial water.

In this beamtime, we carried out Near Edge X-ray Absorption Fine Structure (NEXAFS) measurements on SiO_2 solutions with different concentrations. The NEXAFS measurements were performed at the soft X-ray undulator beamline BL3U at UVSOR-III Synchrotron. In the liquid flow cell, a liquid layer is sandwiched between two 100 nm thick Si_3N_4 membranes with the windows size of 2 × 2 mm^2. Teflon spacers with a thickness of 100 μm are set between the support plates of the Si_3N_4 membranes. Liquid samples are exchangeable *in situ* by using a tubing pump. The temperature of all the liquid samples were controlled at approx. 25°C. The Si_3N_4 membrane window was set to 200 × 200 $μm^2$ to allow for suitable photon fluxes.

In Figure 1 and Figure 2, the O K-edge NEXAFS results are presented. The pure water case is also included in both panels as reference spectra. The spectra exhibit three features: pre-edge (~535 eV), main-edge (~537 eV), and post-edge (~540 eV). The spectrum lines were normalized to the maximum at the pre-edge (Fig. 1) and the post-edge (Fig. 2), which is to take into account variations in the sample thickness. The post-edge intensities of the SiO_2 solutions are higher than those of pure water, which is similar to the existing literature on the study of interfacial water on nanodiamonds [5]. The absorption intensities increase with the increase of the concentration of SiO_2 solutions. This can be linked with the accumulation of hydrated Na^+ ions as concentration of the particles in the suspension increases. The pre-edges have been zoomed in and displayed in the inset (Fig. 2). The intensity of the pre-edge peak is weaker for SiO_2 solutions, have smaller sizes than pure water. Moreover, the intensities have a tendency to decrease with the increase of concentration, which may be affected by the strength of hydrogen bonds between the water layers.

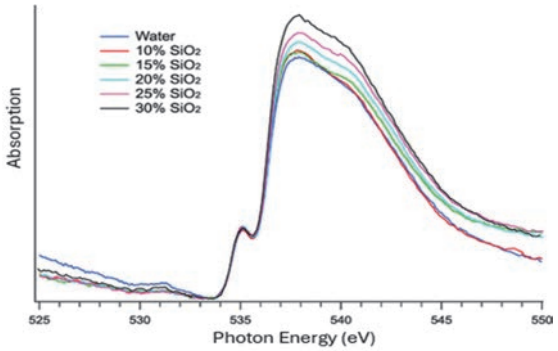

Fig.1. O K-edge NEXAFS spectra of pure water and SiO_2 solutions with different concentrations. The temperatures are around 25°C. The spectra were normalized to the maximum at the pre-edge.

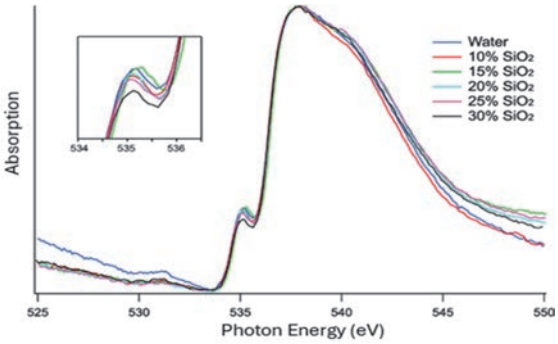

Fig.2. O K-edge NEXAFS spectra of pure water and SiO_2 solutions with different concentrations. The temperatures are around 25 °C. The spectra were normalized to the maximum at the post-edge. The insets zoom in the pre-edge regions.

[1] S.V. Ruffle *et al.*, J. Am. Chem. Soc. **124** (2002) 565.
[2] J. Velasco-Velez *et al.*, Science **346** (2014) 831.
[3] K.C. Jena and D.K. Hore, Phys. Chem. Chem. Phys. **12** (2010) 14383.
[4] S. Dewan, M.S. Yeganeh and E. Borguet J. Phys. Chem. Lett. **4** (2013) 1977.
[5] Petit, T., *et al.*, J. Phys. Chem. Lett. **6** (2015) 2909.

BL3B

Evaluation of Crystallinity of Substrate Interface Region of Deep Ultraviolet Emitting Zinc Aluminate Thin Film

H. Kominami[1,2,3], A. Adachi[1], R. Ishihara[1], K. Yabe[1], J. Kamikawa[1], T. Sadamori[1], D. Takeya[1], M. Mimura[2], M. Yasuda[2], A. Yokoya[2], N. Yoshimura[2] and S. Kurosawa[4,5]

[1]*Graduate School of Integrated Science and Technology, Shizuoka University,*
[2]*Faculty of Engineering, Shizuoka University,*
[3]*Graduate School of Science and Technology, Shizuoka University,*
[1~3]*3-5-1 Johoku, Chuo-ku, Hamamatsu 432-8651 Japan*
[4]*New Industry Creation Hatchery Center (NICHe), Tohoku University 6-6-10 Aza-Aoba, Aramaki, Aoba-ku, Sendai, Miyagi 980-8579, Japan*
[5]*Faculty of science, Yamagata University, 1-4-12, Kojirakawa-machi, Yamagata 990-8560, Japan*

In the field of sterilization and water purification, conventional sterilization methods using chemicals and heat have concerns about the effects of deterioration, toxicity to the human body, and the effects of resistant bacteria. Therefore, sterilization methods using ultraviolet light are becoming popular. Ultraviolet light around 260 nm is said to have the strongest effect, and mercury lamps and xenon lamps are used as ultraviolet light sources for sterilization. However, its use is undesirable from the viewpoint of environmental impact and luminous efficiency. Therefore, we aimed to apply $ZnAl_2O_4$ as the light-emitting layer of a new ultraviolet light-emitting device for sterilization that has high efficiency, long life, low cost, and low environmental impact, and conducted an evaluation. Currently, we are working on the production of double-insulated electroluminescent (EL) lamps, which are one type of solid-state display element. In order for electrons to be injected from the insulating layer to the light emitting layer, it is necessary that the interface between the insulating layer Al_2O_3 substrate and the light emitting layer $ZnAl_2O_4$ be clear and growing uniformly to the surface. This affects the injection of electrons into the light-emitting layer, the acceleration of electrons by the electric field, the collisional excitation of the luminescent center, and the emission of light, which greatly influences the device characteristics. In this study, we focused on $ZnAl_2O_4$ as a light-emitting layer for a new ultraviolet light-emitting device, fabricated it, and evaluated its structure from the surface to the interface.

On a c-plane sapphire substrate (c- Al_2O_3), he deposited about 300 nm of ZnO by magnetron sputtering, and on top of that he deposited about 25 nm of Al_2O_3 as a cap layer. After sputtering, he fabricated $ZnAl_2O_4$ thin films by annealing (990°C, 50 hours) under atmospheric conditions in a muffle furnace and by thermal diffusion. In addition, the thin film surface of the prepared sample was etched using hydrochloric acid to expose the inside of the film, and its characteristics were evaluated using cathodo-luminescence (CL), thin film X-ray diffraction measurement (XRD), analytical FE-SEM, and transmission.

Figures 1 and 2 show the transmittance curve and an enlarged view of the vicinity of the absorption edge, respectively. It was found that the absorption edge shifts to the shorter wavelength side after about 400 nm. This is due to an increase in the bandgap. $ZnAl_2O_4$ is fabricated by thermally diffusing ZnO on c- Al_2O_3. For this reason, it is thought that Zn diffusion varies and the composition deviates from the stoichiometric composition, resulting in the formation of $ZnAl_2O_4$ (predominantly c- Al_2O_3 with a large band gap) lacking Zn.

The results of CL, XRD, and transmittance measurements show that uniform $ZnAl_2O_4$ is formed up to 400 nm inside the sample, but it is thought that $ZnAl_2O_4$ is insufficiently formed further inside.

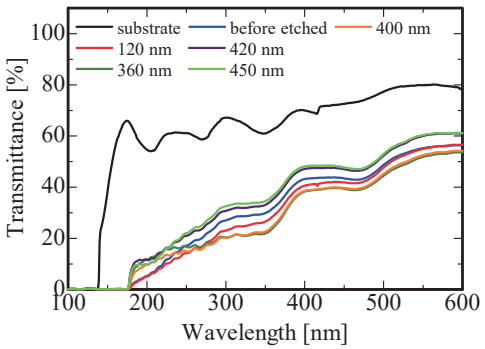

Fig. 1. Transmittance of the etched samples.

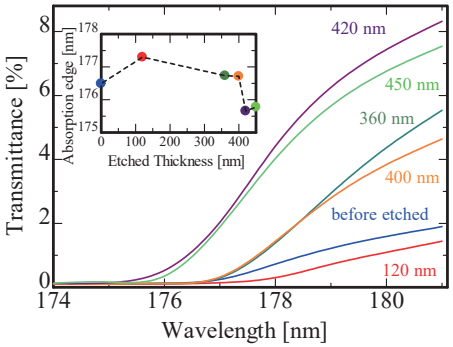

Fig. 2. Absorption edges and etched thickness vs. absorption edge relationship.

BL4B

Interfacial Lattice Strain Induced Spin Reorientation Transition in Pd/Ni Thin Film Heterostructures

T. Miyamachi[1,2], K. Tsutsui[1], H. Ono[1], O. Ishiyama[3,4], T. Yokoyama[3,4] and M. Mizuguchi[1,2]
[1]*Department of Materials Science and Engineering, Nagoya University, Aichi 464-8603, Japan.*
[2]*Institute of Materials and Systems for Sustainability (IMaSS), Nagoya University, Aichi 464-8601, Japan.*
[3]*Institute for Molecular Science, Myodaiji-cho, Okazaki 444-8585, Japan*
[4]*The Graduate University for Advanced Studies, Myodaiji-cho, Okazaki 444-8585, Japan*

The emergence of novel functionality in thin-film heterostructures strongly rely on the interfacial conditions such as lattice strain, mixing or alloying. For the thin film heterostructure composed of magnetic materials, structural modifications at the interface drastically change the degrees of the magnetic coupling, characterizing magnetic properties of the whole system [1]. In this work, we investigate structural, electronic, and magnetic properties of Pd/Ni thin film heterostructures by low energy electron diffraction (LEED) and x-ray absorption spectroscopy/magnetic circular dichroism (XAS/XMCD). To fabricate Pd/Ni thin film heterostructures, we first grow 12 monolayer (ML) Ni thin films on the Cu(001) surface. Then, 2, 6, 14 ML Pd overlayers are grown at room temperature onto Ni/Cu(001). The deposition rates and coverage of Ni and Pd layers are determined by the quartz-crystal microbalance (QCM) and XAS edge jump.

XAS/XMCD measurements are performed at BL4B in UVSOR by total electron yield mode at B = 0 - ± 5 T and T = 7.2 K. The XMCD spectra are obtained at the normal (NI: θ = 0°) and the grazing (GI: θ = 55°) geometries by detecting $\mu_+ - \mu_-$, where μ_+ (μ_-) denotes the XAS recorded at Ni and Pd L adsorption edges with the photon helicity parallel (antiparallel) to the sample magnetization. Note that θ is the angle between the sample normal and the incident x-ray. LEED patterns are checked before XAS/XMCD measurements, to investigate surface lattices of Ni/Cu(001) and Pd/Ni/Cu(001).

We first investigate structural properties of Pd/Ni thin film heterostructures. LEED patterns reveal that both Ni/Cu(001) and Pd/Ni/Cu(001) show p(1×1), indicating epitaxial growth of Ni and Pd layers on Cu(001). We find the surface lattice constant drastically changes by adding Pd overlayers possibly due to the large difference in the lattice constant between fcc Ni and Pd. The coverages of Ni and Pd layers are also evaluated with sub-monolayer accuracy from the ratio of the XAS jump at the L-edge of Ni or Pd to that of Cu [2], ensuring controlled Ni and Pd deposition by the QCM.

Element specific magnetization curves of the Ni layer are recorded by plotting the L_3/L_2 Ni XAS peak intensity as a function of the magnetic field. The magnetization curve of bare Ni layer before Pd deposition shows larger hysteresis loop in the NI geometry than the GI geometry. This clearly reveals the magnetic easy axis towards out-of-plane direction of 12 ML Ni thin films on Cu(001) as previously reported [3]. The impact of Pd overlayers on magnetic properties of the Ni layer is further investigated. We find that the hysteresis loop in the GI geometry becomes prominent with increasing the Pd coverage. At the Pd coverage of 6 ML, the spin reorientation transition (SRT) of the Ni layer from out-of-plane to in-plane direction is observed. The in-plane magnetization of the Ni layer is further stabilized at the Pd coverage of 14 ML. The enhancement of the in-plane magnetic anisotropy is also confirmed from the evaluation of magnetic moments by XMCD sum rules. While the spin magnetic moment is nearly independent of the Pd coverage, the orbital magnetic moment in the GI geometry becomes greater than that in the NI geometry. This indicates the enhanced in-plane magnetic anisotropy of the Ni layer via the spin orbit interaction. Taking the results of LEED observations into considerations, the observed SRT can be explained by the enhancement of lateral lattice constant of the Ni layer with increasing the Pd coverage.

[1] S. Nakashima *et al*., Adv. Funct. Mater. **29** (2019) 1804594.
[2] H. Ono *et al*., J. Phys. Chem. C **127** (2023) 23935.
[3] B. Schulz *et al*., Phys. Rev. B: Condens. Matter **50** (1994) 13467.

BL4B

Stabilizing In-Plane Magnetization of Pd/Ni Thin Film Heterostructures by Interfacial Lattice Strain

T. Miyamachi[1,2], K. Tsutsui[1], H. Ono[1], O. Ishiyama[3,4], T. Yokoyama[3,4] and M. Mizuguchi[1,2]
[1]*Department of Materials Science and Engineering, Nagoya University, Aichi 464-8603, Japan.*
[2]*Institute of Materials and Systems for Sustainability (IMaSS), Nagoya University, Aichi 464-8601, Japan.*
[3]*Institute for Molecular Science, Myodaiji-cho, Okazaki 444-8585, Japan*
[4]*The Graduate University for Advanced Studies, Myodaiji-cho, Okazaki 444-8585, Japan*

Ni thin films grown on Cu(001) are known to exhibit the spin reorientation transition (SRT) with increasing coverage. At the critical coverage of ~ 7 monolayer (ML), the magnetic easy axis changes from in-plane to out-of-plane direction [1]. The SRT of this system is dominantly attributed to modifications of electronic structures near the Fermi energy caused by the tetragonal distortion of the topmost Ni layer via magnetoelastic coupling. We have recently revealed the SRT of 12 ML Ni thin films on Cu(001) from the out-of-plane to in-plane direction by adding Pd overlayers [2]. The in-plane magnetization of the Ni layer is gradually stabilized with increasing the coverage of Pd overlayers and the SRT occurs at the Pd coverage of 6 ML. The SRT of the Ni layer in Pd/Ni thin film heterostructures could be induced by in-plane tensile lattice strain derived from the large difference in the lattice constant between fcc Ni and Pd.

In this work, we grow 6 ML Ni thin film on Cu(001) with magnetic easy axis toward in-plane direction and additionally fabricate Pd/Ni thin film heterostructures with 2, 7, 11 ML Pd overlayers. We investigate the impact of in-plane tensile lattice strain from the Pd layer on the stability of in-plane magnetization of the Ni layer by soft x-ray absorption spectroscopy/magnetic circular dichroism (XAS/ XMCD). Ni and Pd layers are deposited onto Cu(001) at room temperature in ultrahigh vacuum. The deposition rates and coverage of Ni and Pd layers are crosschecked by the quartz-crystal microbalance (QCM) and XAS edge jump [3].

XAS/XMCD measurements are performed at BL4B in UVSOR by total electron yield mode at B = 0 - ± 5 T and T = 7.7 K. The XMCD spectra are obtained at the normal (NI: θ = 0°) and the grazing (GI: θ = 55°) geometries by detecting $\mu_+ - \mu_-$, where μ_+ (μ_-) denotes the XAS recorded at Ni L adsorption edge with the photon helicity parallel (antiparallel) to the sample magnetization. Note that θ is the angle between the sample normal and the incident x-ray. Element specific magnetization curves of the Ni layer are also recorded by plotting the L_3/L_2 Ni XAS peak intensity as a function of the magnetic field.

We first characterize magnetic properties of 6 ML Ni thin films on Cu(001). While no remanence is observed for the magnetization curve recorded in the NI geometry, we confirm a clear hysteresis loop for that in the GI geometry, which reveals in-plane magnetic easy axis of 6 ML Ni thin films as previously reported [1]. With the help of the element specificity of XAS, magnetization curves of the Ni layer in Pd/Ni thin film heterostructures can be extracted. A remarkable change is observed for the magnetization curve recorded in the GI geometry. We find that the coercivity of the Ni layer drastically increases at the Pd coverage of 2 ML, which can be explained from the in-plane tensile lattice strain by Pd overlayers as seen in similar system [2]. It is also important to note that the coercivity of the Ni layer is almost unchanged even when the Pd coverage is increased up to 7, and 11 ML. These results suggest that adding Pd overlayers stabilize the in-plane magnetization of the Ni layer, but the electronic modification of the Ni layers is completed at the Pd coverage of 2 ML.

In the future, we will perform real-space and atomic-scale observations of Pd/Ni heterointerface using scanning tunneling microscopy to investigate the origin of stabilized in-plane magnetization of the Ni layer in Pd/Ni thin film heterostructures [4].

[1] B. Schulz *et al*., Phys. Rev. B: Condens. Matter **50** (1994) 13467.
[2] UVSOR Activity Report **51** (2024) 150.
[3] H. Ono *et al*., J. Phys. Chem. C **127** (2023) 23935.
[4] S. Nakashima *et al*., Adv. Funct. Mater. **29** (2019) 1804594.

BL4B

XMCD Measurements on van der Waals Magnets

R. Ichikawa[1], T. Miyamachi[2], H. Ishii[1], W. Wulfhekel[3], A.-A. Haghighirad[3], O. Ishiyama[4], H. Iwayama[4], E. Nakamura[4], T. Yokoyama[4] and T. K. Yamada[1,5]

[1]*Department of Materials Science, Chiba University, 1-33 Yayoi-Cho, Inage-ku, Chiba 263-8522, Japan*
[2]*Institute of Materials and Systems for Sustainability, Nagoya 464-8603, Japan*
[3]*Institute for Quantum Materials and Technologies, Karlsruhe Institute of Technology, Karlsruhe 76021, Germany*
[4]*Department of Materials Molecular Science, Institute for Molecular Science, Okazaki, Aichi 444-8585, Japan*
[5]*Molecular Chirality Research Centre, Chiba University, 1-33 Yayoi-cho, Inage-ku, Chiba 263-8522, Japan*

The van der Waals (vdW) magnet is a two-dimensional (2D) magnet with magnetic properties even at the thickness of a single atomic layer. It has garnered significant interest as a highly durable and flexible next-generation spintronics material, similar to graphene, which can be peeled off to atomic layer thickness.

In this study, we aim to elucidate interlayer magnetic coupling between heterogeneous magnetic atomic layers using this novel 2D magnet. Understanding interlayer magnetic coupling has been a longstanding research challenge in magnetism. One of the most ideal systems for this is the combination of ferromagnetic Fe(001) and antiferromagnetic Mn(001). Through the efforts of many researchers, including the applicant, over the past 20 years, it has been revealed that a single atomic layer of Mn(001) on ferromagnetic Fe(001) exhibits ferromagnetic 0° coupling between adjacent Mn atoms within the layer and antiferromagnetic 180° coupling between layers. However, this interlayer antiferromagnetic coupling arises from the fourth layer of Mn. The magnetic coupling from the first to the third layers remains unclear, attributed to strong electronic interactions at the Fe/Mn interface, leading to various effects such as mixing of Fe and Mn and crystalline strain at the interface, resulting in a simultaneous alteration and disorder of the spin-polarized electron structure. Consequently, the magnetic moment is also altered and disturbed, leaving the magnetic coupling at the interface of the original Fe and Mn atomic layers unresolved. Despite extensive theoretical calculations on Mn/Fe(001) systems, the conclusions have been limited to indicating the possibility of various magnetic structures.

This study aims to put an end to this longstanding mystery by utilizing one of the vdW magnets named Fe_3GeTe_2 (FGT). To extract the pure magnetic coupling between Fe and Mn atomic layer films, a decoupling layer that cuts off the electronic interaction between the two films is required. Atomic layer magnets function with halogen or chalcogen element films on both sides of the magnetic atomic layer as decoupling layers. Therefore, we employ this Fe-based atomic layer magnet as a substrate. While applying an in-plane and out-of-plane magnetic field, X-ray absorption spectroscopy (XAS) and X-ray magnetic circular dichroism (XMCD) measurements are conducted to obtain magnetic hysteresis curves and extract the pure magnetic coupling of Fe and Mn atomic layer films.

We brought three FGT single crystals and attached them to the sample holder of the XMCD apparatus. Since the crystals were small, with sizes of 2-3 mm, and there was a possibility that the beam might not hit them, we aligned three of them vertically. Care was taken to ensure that the adhesive did not overflow from the samples as they were cured. A copper holder was used. From XPS measurements, if an iron peak rather than a copper peak appeared, it would indicate that the beam was hitting the FGT sample. XPS peak measurements were conducted while changing positions.

Vacuum cleavage using the XMCD apparatus was also conducted. Although FGT is an atomic layered material, it exhibits metallic properties, and it had been confirmed from prior research that impurities would adsorb on the surface when exposed to air. Therefore, we directly attached Scotch tape to the sample in the atmosphere and made loops with the tape. In a vacuum, we attempted cleavage by pulling the loops with a transfer rod. However, when we tried to delaminate all three samples with one tape, some samples were successfully cleaved, while others were not completely cleaved due to differences in sample height. Therefore, we cut the end of the tape into three parts to allow each tape to adhere to the sample surface and enable vacuum cleavage for each.

After the vacuum cleavage, the sample holder was set in the XMCD apparatus. It was cooled down to 5 K using liquid nitrogen and helium. XPS measurements were performed while changing the magnetic field. The incident angle of light to the sample was changed, and magnetization curves in-plane and out-of-plane were measured. Magnetization curves showed hysteresis when ±5 Tesla (T) was applied, confirming ferromagnetism at 5 K. Prior research suggested that FGT could exhibit unique magnetic structures, such as skyrmions within lower fields. Thus, we extensively measured the magnetization changes within ±500 mT.

The beam time ended before we could conduct magnetization curve measurements of Mn on FGT due to the time required for vacuum cleavage expertise. We hope to attempt it next time.

BL4B

Charge Transfer in Solution-Mixed and Sequential Doping P3HT:F4-TCNQ Films by NEXAFS Spectroscopy

Y. Hoshi [1] and K. K. Okudaira [2]
[1]*Graduate School of Science and Technology, Chiba University, Chiba 263-8522, Japan*
[2]*Graduate School of Engineering, Chiba University, Chiba 263-8522, Japan*

As high-performance organic semiconductors, π-conjugated polymers have attracted much attention due to their charming advantages including low-cost, solution processability, mechanical flexibility, and tunable optoelectronic properties [1]. The electrical conductivity of semiconducting polymers can be effectively tuned over several orders of magnitude by doping with not only inorganic materials such as iodine, but also organic molecule such as F4-TCNQ. Molecular dopants such as F4-TCNQ undergo ground–state charge transfer with their host semiconductor, yielding polarons or bipolarons on the semiconductor. There are multiple different methods for producing doped polymer films, (1) evaporation of dopant in vacuum, (2) casting a film of pre-doped polymer created by blending the polymer and dopant in solution, which we refer to as mixed solution doping, (3) casting a film of dopant on pre-coated polymer film, which we refer to as sequential solution doping [2,3]. We evaluate the doping efficiency (charge transfer process) in P3HT doped with F4-TCNQ by mixed and sequential solution method using NEXAFS spectroscopy.

The mixed solution doping method: F4-TCNQ in chlorobenzene (CB) with 0.1mg/ml and 1.0mg/ml and P3HTare mixed and quickly spin coated to form a film on ITO substrate. The sequential solution doping method: undoped P3HT films are first spin coated from CB on ITO substrate. Once dried, the films are doped by the spin casting with a solution of F4-TCNQ. NEXAFS spectra of the P3HT doped with F4-TCNQ using total electron yield (TEY) modes were measured at the beamline 4B of the UVSOR in the Institute of Molecular Science.

Figure 1 shows N K-edge NEXAFS spectra of P3HT sequential and mixed doped with F4-TCNQ by using different F4-TCNQ concentrations. The N K-edge NEXAFS of P3HT doped F4TCNQ consist of peaks A - C. The spectral feature of the samples by mixed doping process both using 0.1 mg/ml and. 1.0 mg/ml CB solution are similar to those of F4-TCNQ films by deposition on Si(100) [4]. These peak structures are comparable to those reported in TCNQ thin films. According to the peak assignment of pure TCNQ, peak A is assigned to π* orbitals (LUMO), peak B to π* and σ*, and peak C to π* [4]. N K-edge NEXAFS spectra of P3HT sequential doped with F4-TCNQ strongly are modified compared to that of mixed doped with F4-TCNQ. It is noted that the intensities of peak A (LUMO) and C decrease in sequential doped spectrum. The decrease in the intensity of peak A is interpreted to be the result of charge transfer from the P3HT to the LUMO of the acceptor molecule (F4-TCNQ). As shown in Fig.1 (b) the energy position as well as the spectral shape of the intense peak B in N K-edge NEXAFS of P3HT sequential doped with F4-TCNQ are different from those of mixed-doped ones. It is proposal that by using sequential doping, the charge transfer occurs initially by charging the cyano groups, then the local structure around cyano groups would change.

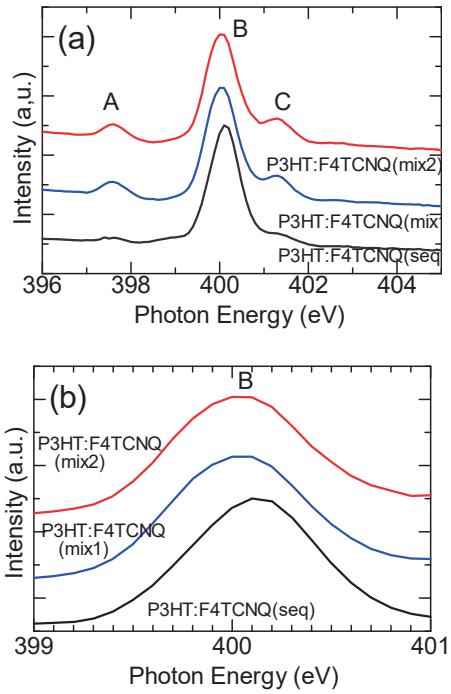

Fig. 1. (a) N K-edge NEXAFS spectra of P3HT sequential doped and mixed doped with F4-TCNQ (mix1: mixed with F4-TCNQ using 0.1 mg/ml CB solution. mix2: 1.0mg/ml CB solution). (b) enlargement of N K-edge NEXAFS spectra of P3HT sequential doped and mixed doped with F4-TCNQ at hv from 399 eV to 401 eV.

[1] X. Guo *et al*., Prog. Polym. Sci. **38** (2013) 1832.
[2] M. T. Fontana *et al*., J. Phys. Chem. C **123** (2019) 22711.
[3] Y. Yoshimoto *et al*., Org. Electron. **15** (2014) 356.
[4] J. Fraxedas *et al*., Phys. Rev. B: Condens. Matter **68** (2003) 195115.

Angle-Resolved Photoemission Circular Dichroism for Chiral Molecule Overlayer on Monolayer WS_2

F. Nishino[1,2], K. Fukutani[1,2], P. I. Jaseela[1,2], J. Brandhoff[3], F. Otto[3], M. Grünewald[3], M. Schaal[3], J. Picker[4], Z. Zhang[5], A. Turchanin[4], S. Makita[6], H. Iwayama[6], T. Hirose[5], T. Fritz[3] and S. Kera[1,2,6]

[1]*Institute for Molecular Science, Okazaki 444-8585, Japan*
[2]*School of Physical Sciences, The Graduate University for Advanced Studies, Okazaki 444-8585, Japan*
[3]*Institute of Solid State Physics, Friedrich Schiller University Jena, Helmholtzweg 5, Jena 07743, Germany*
[4]*Institute of Physical Chemistry, Friedrich Schiller University Jena, Lessingstraße 10, Jena 07743, Germany*
[5]*Institute for Chemical Research, Kyoto University, Gokasho, Uji, Kyoto 611-0011, Japan*
[6]*UVSOR Synchrotron Facility, Institute for Molecular Science, Okazaki 444-8585, Japan*

A chirality-induced spin selectivity (CISS) effect with controlled chiral molecules on various solid surfaces has been actively studied for various applications, such as for spintronics and enantio-separations [1]. On the other hand, many aspects of this phenomenon, including its mechanism underlying its extraordinarily large spin polarization effects, remain unknown.

Our approach to this challenge is to fabricate well-defined chiral molecular systems on solid surfaces with known spin-polarized electronic band structures, and to investigate how the surface chirality affects the emitted electrons from the solid by angle-resolved photoemission spectroscopy (ARPES).

As a preliminary study, in this work, we used angle-resolved photoemission circular dichroism (CD-ARPES) for the system of chiral molecular overlayer on achiral substrate possessing fully spin-polarized electrons to assess how the electrons emitted from the substrate recognize the surface chirality.

The enantiopure chiral molecule, thiadiazole-[9] helicene (TD[9]H) [2], was used in this study as show in Fig. 1(a). The substrate used was a monolayer WS_2/Au(111) (ML-WS_2) with fully spin-polarized bands at $\bar{K}$' and $\bar{K}$ points [3]. After depositing the enantiopure TD[9]H on the ML-WS_2 under ultra-high vacuum condition, low-energy electron diffraction (LEED) showed an ordered molecular overlayer with broken mirror-symmetry, indicating the surface chirality has been induced on the system.

Following the confirmation of the surface chirality, CD-ARPES measurements were performed, using left circularly polarized (LCP) and right circularly polarized (RCP) lights for both the clean substrate and the (*M*)-TD[9]H/ML-WS_2 samples, as shown in Fig. 1(b).

Figures 1(c)-(e) show the CD-ARPES maps obtained for clean ML-WS_2 substrate. It can be seen that the dichroic signals at the $\bar{\Gamma}$-$\bar{M}$plane [black dotted lines in Figs. 1(c), 1(d) and the entire map in Fig. 1(e)], which is the mirror plane of the substrate, is very weak. Furthermore, the dichroic signals in the $\bar{\Gamma}$-$\bar{K}$ and $\bar{\Gamma}$-$\bar{K}'$ directions are seen to be generally anti-symmetric with respect to the $\bar{\Gamma}$-$\bar{M}$ plane.

These characteristics of dichroic signals from substrate can readily be understood from the point of view of symmetry. Since the substrate is achiral and the mirror plane of the crystal coincides with the plane of light incidence, it must hold that $I_{RCP}(k_x, k_y) = I_{LCP}(-k_x, k_y)$ (Equation 1), where I_{RCP} and I_{LCP} are the photoelectron intensities with RCP and LCP lights, respectively. That is, the achirality of substrate is reflected in our CD-ARPES results.

Next, the CD-ARPES results after the deposition of (*M*)-TD[9]H are shown in Figs. 1(f)-(h). Unlike the CD-ARPES results from the clean substrate, finite (blue) dichroic signals were observed uniformly in the substrate bands, molecular orbitals and inelastic scattering regions even in the E-k slice of the $\bar{\Gamma}$-$\bar{M}$ plane as can be seen in Fig. 1(h). While more investigations are necessary, the apparent violation of equation 1 above could arise from the loss of achirality (i.e., emergence of chirality) for the electrons in the system of chiral molecular overlayer on achiral substrate.

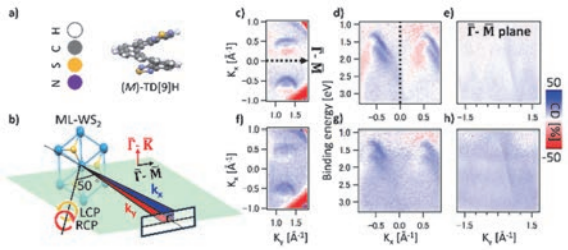

Fig. 1. (a) Molecular structures of (*M*)-TD[9]H. (b) Schematic illustration of CD-ARPES setup. The relative orientations of the sample and the photoelectron analyzer slit are shown. (c)-(e) CD-ARPES map of ML-WS_2. (f)-(h) CD-ARPES map of (*M*)-TD[9]H/ML-WS_2. (c) and (f) shows constant-energy cut and (d), (g) is the intensity plots in E-k_x slice. (e) and (h) is the intensity plots in E-k_y slice.

[1] S.-H. Yang *et al*., Nat. Rev. Phys. **3** (2021) 328.
[2] Z. Zhang *et al*., Tetrahedron **142** (2023) 133514.
[3] P. Eickholt *et al*., Phys. Rev. Lett. **121** (2018) 136402.

BL4B

Photoemission Spectroscopy Measurement on Germanium Incorporated Carbon-Based Nanoribbon Structures

K. Sun[1,2], K. Fukutani[3], S. Kera[3] and S. Kawai[2,4]

[1]*International Center for Young Scientists, National Institute for Materials Science, 1-2-1 Sengen, Tsukuba, Ibaraki 305-0047, Japan*

[2]*Center for Basic Research on Materials, National Institute for Materials Science, 1-2-1 Sengen, Tsukuba, Ibaraki 305-0047, Japan*

[3]*Department of Photo-Molecular Science, Institute for Molecular Science, Okazaki 444-8585, Japan*

[4]*Graduate School of Pure and Applied Sciences, University of Tsukuba, Tsukuba 305-8571, Japan*

Germanium(Ge) belongs to both the carbon group and metallic elements with the atomic number 32, with four valence electrons for allowing the formation of multi covalent bonds[1]. Carbon-based nanomaterials with atomic precision are viewed as a candidate for the application in next-generation nanoelectronics. Doping Ge into carbon nanostructures may potentially modify their electronic structures. It is significant to fabricate Ge-incorporated carbon-based nanostructures by C-Ge coupling for providing a material foundation.

We present fabrication of Ge incorporated carbon nanoribbon structures. Molecules 1,4,5,8-tetrabromonaphthalene **1** was employed as a precursor to react with Ge atoms on Ag(111). The reaction processes were illustrated in Fig. 1, distinct from C-Si coupling on Au(111)[2,3]. **1** were deposited on Ag(111), subsequently formed organometallic chains with Ag adatoms by debromination after annealing at 150 ℃. Next, Ge were deposited on the Ag(111) surface and subsequent annealing at 200 ℃ results in the formation of Ge-incorporated nanostructure structures.

In order to demonstrate the nanoribbon structures containing Ge atoms, we performed photoemission spectroscopy measurement by using BL4B of UVSOR. Figure 2 shows the experimental results. Scanning tunneling microscopy (STM) topography (Fig. 2a) of Ag-organic oligomers and Ge clusters were seen on Ag(111) before annealing at high temperature. The corresponding Ge 3d curves show spin–orbit doublet peaks of $3d_{5/2}$ (30.85 eV) and $3d_{3/2}$ separated by 0.59 eV (Fig. 2b). Next, the sample was heated at 200 ℃ for reaction between Ag-organic chains and Ge atoms. The STM topography shows Ge incorporated nanoribbon structures (Fig. 2c). The corresponding Ge 3d curve became quite complex. After careful analysis, we found three sets of doublet peak components, which can be associated to three different charge states of the Ge atom. Among them, the red doublet peaks exhibit higher binding energy compared to the original peaks, indicating the presence of C-Ge-C bonds on Ag(111). The green doublet peaks with lower binding energy may originate from AgGe alloy. These results demonstrated that we have successfully fabricated Ge-incorporated nanoribbon structures.

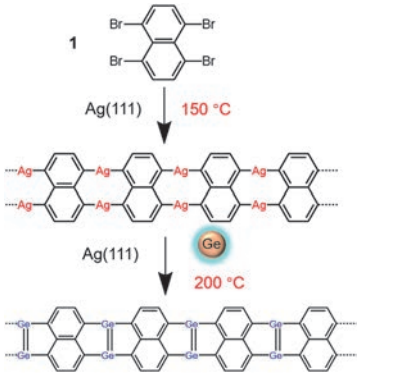

Fig. 1. Scheme of synthesis of Ge-incorporated nanoribbon structure on Ag(111).

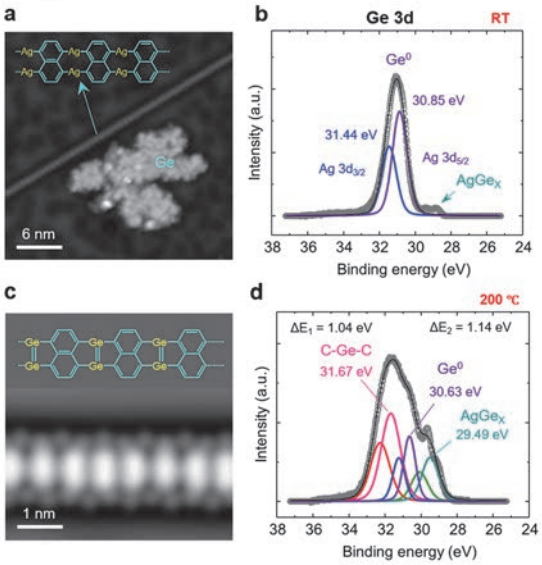

Fig. 2. Photoemission spectroscopy measurement on Ge-incorporated nanoribbons.

[1] M. L. Amadoruge and C. S. Weinert, Chem. Rev. **108** (2008) 4253.
[2] K. Sun *et al*., Nat. Chem. **15** (2023) 136.
[3] K. Sun *et al*., Angew. Chem. Int. Ed. **Early View** (2024), e202401027.

BL5U

Geometry-Induced Photoelectron Spectroscopy from Si{111} Facet Surfaces on Three-Dimensionally Fabricated Facet-Lined Structures

K. Hattori[1], Ni'matil Mabarroh[1], Juharni[1], Y. Kimoto[1], Y. Kitagawa[1], K. Tsubosaki[1], R. M. Tumbelaka[1], S. Tanaka[2], A. N. Hattori[2], S. Suga[2] and K. Tanaka[3]

[1]*Nara Institute of Science and Technology, Ikoma 630-0192, Japan*
[2]*SANKEN, Osaka University, Ibaraki 567-0047, Japan*
[3]*UVSOR Synchrotron Facility, Institute for Molecular Science, Okazaki 444-8585, Japan*

Highly controlled three-dimensional (3D) structures will promise to become the platform for novel properties originated from the electronic states at local surfaces and edges based on the 3D geometries. Recently, our group has successfully created 3D-Si surfaces by combining lithography and surface treatment techniques [1], and reported a successful creation of Si{111}7×7 clean facet surfaces showing surface and bulk electronic bands using angle-resolved photoelectron spectroscopy (ARPES) [2, 3], and also film bands of √3×√3-Ag ultra-thin film on Si{111} [3], aiming for a future 3D-surface band-engineering.

The previous all ARPES measurements for the 3D-Si surfaces were limited for the symmetric electronic band structures around $\bar{\Gamma}$ point toward the normal orientation of the Si{111} facet surfaces [2, 3]. In order to approach unique electronic states arising from 3D geometrical surfaces and edges, at first, we need to understand the fundamental effect of 3D sample geometry on ARPES, for instance, 1) co-existence of bands from different 3D structure surfaces and 2) shadow effect of 3D hinderance for photo irradiation, which we expect. Thus, here we focused on how 3D structure effects appear in ARPES measurements.

In order to study 3D geometrical factors in ARPES, we surveyed rotation angle dependence using facet line standard Si{111} facet surfaces on a (001) substrate. In addition, we selected √3×√3-Ag ultra-thin films on Si{111}, because they lead to clear and simple bands at highly symmetric $\bar{\Gamma}^{1\times1}$ and $\bar{K}^{1\times1}$ points 1×1 unit, which allows easy to distinguish bands of different 3D facet surfaces.

In experiment, 3D Si facet-lined structures with (111) and $(\bar{1}\bar{1}1)$ facet surfaces with the facet angle of 55° and facet pitch of 4 μm period, were prepared by using a photo-lithography and wet etching followed by an RCA treatment. In UVSOR BL5U vacuum, the sample was degassed, flashed, and deposited by Ag of ~10 monolayer at 770 K. The superposition of double faceted √3×√3 low-energy electron diffraction patterns [3] were observed at room temperature (RT).

The band structures for the 3D-Si{111}√3×√3-Ag facet surfaces at RT were measured with *p*-polarized photons of surface sensitive 60 eV having 58° angle to the electron detector. The band mapping was conducted with the *x* and *y* emission angle of -15° to +15°, the binding energy E_B of -0.25 eV to +1.47 eV, and the capturing time of 1 hour for each map. The Fermi level was referred to the Au results. The band maps near Fermi level depending on the displayed rotation angle θ was monitored.

Figure 1(a) shows the map at θ = +5° displaying 4 clear circles corresponding to electron-pocket bands at $\bar{K}_{3L}^{1\times1}$ and $\bar{K}_{3R}^{1\times1}$ originated from the left and right facet surfaces, respectively; the simple schematics in real and reciprocal spaces are shown in Figs. 1(c) and 1(d), respectively. Here we confirmed the superimpose of the bands from different 3D-Si facet films, as expected.

However, we notice the right facet is shadow for the incident photons as illustrated in Fig. 1(b), leading to no photoelectrons at $\bar{K}_{3R}^{1\times1}$. The appearance of photoelectrons at $\bar{K}_{3R}^{1\times1}$ implies photo "reflection" due to the 3D structure becomes dominate, out of the first expectation. Indeed, we found both diffused and specular photo reflections affect in 3D samples ARPES, from the θ dependence of the photoelectrons at $\bar{K}_{3L}^{1\times1}$ and $\bar{K}_{3R}^{1\times1}$ (Fig. 1 (b)) compared to the simulation in a simple reflection model.

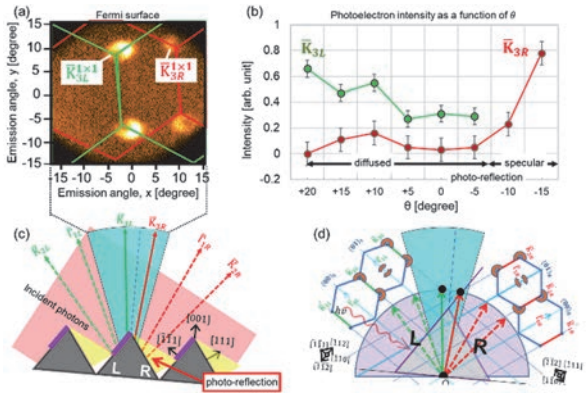

Fig. 1. (a) ARPES map of 3D-Si{111}√3×√3- Ag facet surfaces at θ = +5°, displaying the Fermi bands at $\bar{K}^{1\times1}$ points originated from different left and right facet surfaces. (b) Photoelectron intensities of $\bar{K}_{3L}^{1\times1}$ and $\bar{K}_{3R}^{1\times1}$ bands as a function of θ. (c) Schematic in real space. The orange is the incident photons, and the yellow is photo reflected area. Positive θ corresponds to the sample CW rotation. (d) Schematic in reciprocal space. The purple arc is the Ewald sphere of the Fermi level electrons, and cyan lines are the reciprocal lattice rods.

[1] A.N. Hattori *et al*., Surf. Sci. **644** (2016) 86.
[2] K. Hattori *et al*., e-J. Surf. Sci. Nanotechnol. **30** (2022) 214.
[3] K. Hattori *et al*., UVSOR Activity Report **50** (2023) 155.

BL5U

Van Hove Singularity Induced by an Interfacial Metallic Layer in Ca-Intercalated Bilayer Graphene on SiC

S. Ichinokura[1], K. Tokuda[1], M. Toyoda[1], K. Tanaka[2], S. Saito[1] and T. Hirahara[1]
[1]*Department of Physics, Tokyo Institute of Technology, Tokyo 152-8551, Japan*
[2]*UVSOR Synchrotron Facility, Institute for Molecular Science, Okazaki 444-8585, Japan*

Graphene-based superconductors hold great promise for a wide range of applications due to their optical transparency, mechanical robustness, and flexibility. Among these materials, C_6CaC_6, a bilayer graphene intercalated with calcium, exhibits the highest critical temperature (T_c) [1,2]. Early investigations predominantly embraced the concept of a free-standing C_6CaC_6 model, grounded in its observed electronic structure. However, recent propositions have suggested intercalation at the interface of C_6CaC_6 and the SiC substrate [3], although the interface configuration at elevated calcium density remains unexplored, potentially giving rise to unconventional electronic structures such as saddle points and van Hove singularities (VHS) [4].

In this study, we have elucidated that the introduction of high-density calcium induces intercalation at the interface, resulting in the confinement epitaxy of a metallic calcium layer beneath C_6CaC_6. Notably, the hybridization of the interface band and one of the Dirac cones leads to the emergence of a novel electronic phase, wherein a distinctive VHS enhances the density of states near the Fermi level.

C_6CaC_6 samples were synthesized through the deposition of calcium on epitaxial graphene atop a 4H-SiC(0001) substrate maintained at 300 °C. The calcium density within the specimen was quantified using the unit of ML (= 6.3×10^{14} cm^{-2}). The band structure was explored via angle-resolved photoemission spectroscopy using a He lamp (hν = 21.2 eV) and synchrotron radiation (hν = 33 eV) at BL5U.

In Figs. 1(a) and (b), we present the band structure of the current system at the 1.2 and 2.5 ML stages, corresponding to low and high calcium density stages, respectively. At 1.2 ML, three sets of metallic bands can be identified around the Γ point: a parabolic interlayer band (IL) and Dirac cones (α* and β*) folded from the K point due to the formation of $\sqrt{3}\times\sqrt{3}$ Brillouin zone (BZ). These electronic states are characteristic of free-standing C_6CaC_6 [5]. At 2.5 ML, as depicted in Fig. 1(b), an X-shaped metallic band appears at the M* point in $\sqrt{3}\times\sqrt{3}$ BZ, which deviates from the free-standing model. By electron diffraction and core-level photoemission, we have revealed that the band is an interfacial metallic band (IFM) originating from the epitaxial layer of calcium at the interface of C_6CaC_6 and SiC. Around the Fermi level, IFM hybridizes with the β* band. Graphene's original saddle point at the M point of the BZ is replicated at the M* point in the $\sqrt{3}\times\sqrt{3}$ BZ. At the 1.2 ML stage, the saddle point of the β* band lies slightly above the Fermi level. At the 2.5 ML stage, the β* band connects to IFM through hybridization, giving rise to a hole-like dispersion with a maximum at the Fermi level.

The vertex of the hole band has been validated as a saddle point via the scrutiny of electron-like dispersion along the orthogonal direction in our high-resolution measurements. Figures 1(c)-(e) depict k_x dispersion at k_y = -0.75, -0.63, and -0.50 Å^{-1}. The electron-like arrangement in Fig. 1(e) and (c) unequivocally illustrates that the diminutive Fermi surface depicted in Fig. 1(d) constitutes a saddle point, where the VHS occurs.

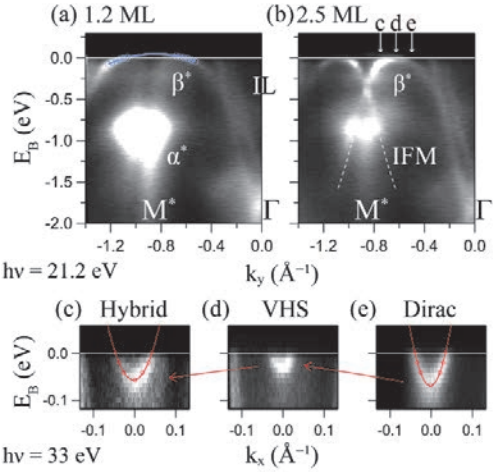

Fig. 1. (a) and (b) depict ARPES spectra along the Γ-M* direction at Ca density of 1.2 and 2.5 ML, respectively. The blue circles and solid line in (a) represent the set of (E, k_y) points of β* band and parabolic fitting to it, respectively. The dashed white lines in (b) delineate the IFM bands. In (c), (d), (e), electronlike band dispersion high-Ca-density-state along k_x direction is highlighted. Measurement cuts (k_y = -0.75, -0.63, and -0.50 Å^{-1}) are indicated by white arrows in (b).

[1] S. Ichinokura *et al.*, ACS Nano **10** (2016) 2761.
[2] X. Wang *et al.*, Nano Lett. **22** (2022) 7651.
[3] H. Toyama *et al.*, ACS Nano **16** (2022) 3582.
[4] J. L. McChesney *et al.*, Phys. Rev. Lett. **104** (2010) 136803.
[5] K. Kanetani *et al.*, PNAS **109** (2012) 19610.

BL5B

Characterization of Amorphous and Polycrystalline Selenium Thin Films by Vacuum Ultraviolet Absorption Spectroscopy

K. Hayashi

Department of Electrical, Electronic and Computer Engineering, Gifu University, Gifu 501-1193, Japan

It is well-known that various photoinduced phenomena such as changes in optical band gap and conductivity occur in chalcogenide amorphous semiconductors by light irradiation [1]. Although many studies have been done on the photoinduced phenomena of these materials, little is known about the details of these mechanisms. We are investigating the annealing temperature dependence of conductivity changes due to light irradiation on amorphous selenium thin films. We observed a drastic increase in photoconductivity at annealing temperatures above 60°C. This change was confirmed to be due to the phase change from the amorphous structure to the polycrystalline structure from the XRD pattern change and the band gap change. In the previous report [2], we reported on the results of measurements using BL4B of changes in the VUV transmission spectrum of amorphous selenium films before and after light irradiation and after annealing. In this paper, we report the energy structure change due to the phase change from amorphous structure to polycrystalline structure by annealing using VUV absorption spectroscopy.

Sample used for the measurement of the VUV absorption spectra was amorphous selenium thin films prepared onto thin aluminum film by conventional evaporation technique. The sample thickness was about 180nm. The aluminum film of the thickness of 200 nm was used to eliminate the higher order light from the monochromator in the VUV region. These measurements were carried out at room temperature on the BL5B beam line of UVSOR. The spectrum was measured by using the silicon photodiode as a detector. Two pinholes of 1.5mm in a diameter were inserted between the monochromator and sample to remove stray light. The intensity of the VUV light was monitored by measuring the TPEY of a gold mesh. The positions of the core levels for the samples were calibrated by referencing to the 2p core level absorption of the aluminum film. The phase transition from amorphous to polycrystalline structure was achieved by annealing at temperatures above 343 K for a total of 3 hours.

Figure 1 shows the VUV absorption spectra of Se 3d core levels in amorphous and polycrystalline phases. The VUV absorption spectra of the Se 3d core level of the amorphous phase differed slightly from the previous research [3], but absorption peaks were observed at similar energy positions. In both the amorphous and polycrystalline phases, a broad structure with a shoulder around 55 eV has been observed. This broad peak with a shoulder is thought to be due to spin-orbit splitting of the Se 3d level. The absorption peak of the amorphous phase is about 0.15 eV lower than that of the polycrystalline phase. This is because the optical bandgap of the polycrystalline phase is smaller than that of the amorphous phase. As can be seen from the figure, structures appear around 63 eV in the film after crystallization. The origin of this structure remains unknown. However, it may reflect local bonding states resulting from the transition from amorphous to polycrystalline phases. The spectrum obtained after crystallization is broader than the spectrum obtained from the as-deposited amorphous film. The spectrum of as-deposited amorphous films may depend on the preparation conditions of the film. Therefore, further investigation into its details will be necessary in the future. The detailed experiments and analysis will be done in the next step. More detailed experiments are necessary to clarify the origin of the VUV absorption spectra.

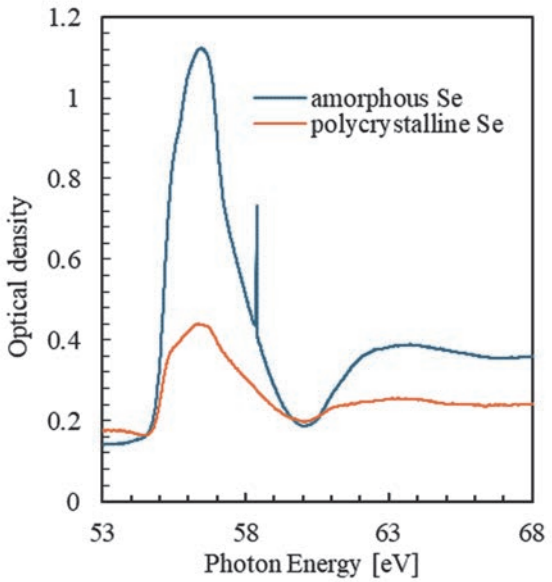

Fig. 1. VUV absorption spectra of Se 3d core levels in amorphous and polycrystalline phases.

[1] K. Tanaka, Rev. Solid State Sci. **4** (1990) 641.
[2] K. Hayashi, UVSOR Activity Report **50** (2023) 152.
[3] J. Bordas and J. B. West, Philos. Mag. **34** (1976) 501.

III-4

BL5B

Electronic Study of Large-Area Hydrogen Boride Sheets by X-ray Absorption Spectroscopy

K. Yamaguchi[1], M. Niibe[1], T. Sumi[1], E. Nakamura[2], K. Tanaka[2,3] and I. Matsuda[1]
[1]*The Institute for Solid State Physics (ISSP), The University of Tokyo, Kashiwa, Chiba 277-8581, Japan*
[2]*UVSOR Synchrotron Facility, Institute for Molecular Science, Okazaki 444-8585, Japan*
[3]*School of Physical Sciences, The Graduate University for Advanced Studies (SOKENDAI), Okazaki 444-8585, Japan*

A hydrogen boride (HB) sheet is a two-dimensional boron material that has shown rich functionalities, such as hydrogen storage [1] and carbon dioxide reduction [2]. In addition, it has also captured interests as an electrically conducting material because of the semi-metallicity, predicted by theoretical calculations [3]. The HB sheet has been so far prepared in the powder form, limiting its applications. Recently, we have succeeded in synthesizing the large area HB sheets and in scrutinizing the electronic states in detail by X-ray absorption spectroscopy (XAS) to examine the technical potential. The experiment was made at BL-5B and XAS spectra were recorded by two detection schemes, the transmission yield and the total electron yield (TEY).

Figure 1(a) shows a photograph, taken during the sample installation to the measurement chamber at the beamline. The HB samples were treated in a glove bag, filled with nitrogen gas, to minimize a possible oxidization of the samples. Figure 1 (b) shows a photograph of the sample holder. It is a combination of a bare metal mesh and the HB-covered mesh to detect I_0 and I, respectively. The TEY signal was detected by the drain current of samples, while the transmission intensity was recorded by a photodiode. The measurement was made at room temperature under the high vacuum condition.

Figure 2 is a collection of XAS spectra of the HB sheet, taken as the transmission intensity and by TEY. Spectral features are identified as labeled with S_1-S_3. The S_2 peak is assigned to boron oxides. The intensity is much smaller compared to the previous report [3], indicating the success synthesis of the high purity samples and appropriateness of the treatments in a glove bag (Fig.1(a)). The peaks, S_1 and S_1', located at photon energy around 190 eV and those, S_3 and S_3', around 200 eV are ascribed to electronic states of the HB sheet. Appearance of the XAS spectra was distinctive between the two detection schemes. Since the transmission method and TEY are bulk- and surface-sensitive, respectively, a set of the spectra provides comprehensive information of electronic states of the HB sample. The experimental spectra will be compared with the simulated spectra by the first principles calculation to unveil origins of the spectral peaks (S_1, S_1', S_3, S_3').

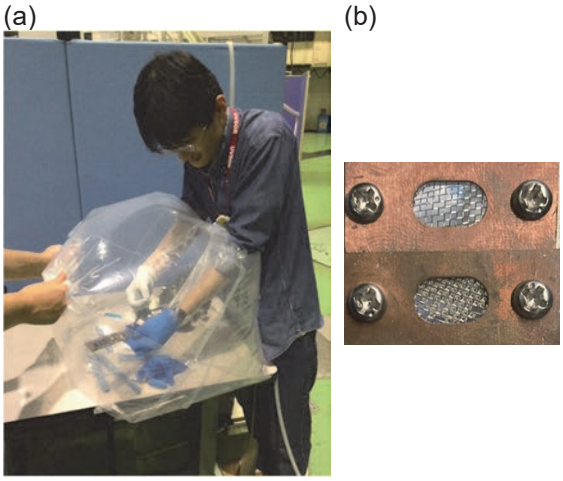

Fig. 1. Photographs of (a) the sample installation and (b) the sample holder. The top is a bare metal mesh and the bottom is with the HB sample.

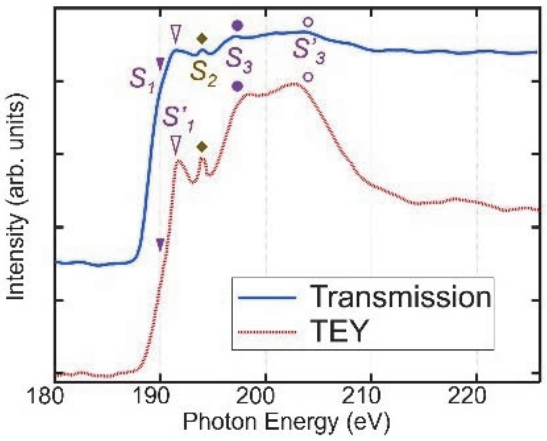

Fig. 2. XAS spectra of HB sheets. The blue curve was taken by the transmission method, while the red one by the TEY method. The spectral features are labeled.

[1] R. Kawamura *et al*., Nat. Commun. **10** (2019) 4880.
[2] T. Goto *et al*., Commun. Chem. **5** (2022) 118.
[3] I. Tateishi *et al*., Phys. Rev. Mater. **3** (2019) 024004.

BL6U

Deposition of High-Quality Ir(111) Thin Films by Molecular Beam Epitaxy

E. Hashimoto[1], Y. Onuma[1], H. Kurosaka[1], Y. Nishio[1], F. Matsui[2] and S. Koh[1]

[1]*Department of Electrical Engineering and Electronics, College of Science and Engineering, Aoyama Gakuin University, 5-10-1 Fuchinobe, Chuo-ku, Sagamihara, Kanagawa 252-5258, Japan*

[2]*UVSOR Synchrotron Facility, Institute for Molecular Science, Okazaki 444-8585, Japan*

Chemical vapor deposition (CVD) is a promising method to synthesize high-quality. large-area, and transferrable graphene. We have investigated low-pressure CVD methods using epitaxial Ir(111)/α-Al_2O_3(0001) substrate with single-crystallinity. We demonstrated the reusability of the Ir(111) substrate and evaluated the single-crystallinity and electronic structure of graphene/Ir(111) [1-4]. Further improvement of the surface flatness and crystallinity of the substrate is effective in further improving the quality of CVD graphene. In this research, we performed the deposition of Ir(111) thin films by molecular beam epitaxy (MBE) and evaluated the quality of Ir thin films by photoelectron momentum microscopy (PMM).

We deposited Ir(111) thin films on α-Al_2O_3(0001) substrates by MBE method. First, the low-temperature buffer layer was deposited with the temperature of the substrate holder set at 500℃ for 20 min. Then, the temperature of the sample holder was raised to 950 ℃ and the Ir(111) thin films were deposited for 220 min. By deposition for a total of 240 min, thin films with a thickness of 70 nm were grown. Afterwards, Ir(111) thin films were annealed under H_2 atmosphere at 1000℃ for 60 min.

Figures 1(a) and (b) show the XRD diffraction for the Ir layers deposited on α-Al_2O_3(0001). Diffraction peaks caused by Ir(111) and α-Al_2O_3(0001) were observed in the 2theta/omega profile (Fig.1(a)). The XRD pole figure along Ir[111] is shown in Fig. 1(b). The observed Bragg peaks for Ir{111} have 6-fold symmetry. These ideally have 3-fold symmetry, thus indicating that Ir(111) thin films had twin domains. Figure 1(c)-(e) show the Fermi surface of Ir(111) thin films. Photon energy was set to 100 eV. At the observation position moving 100 μm from the position of Fig. 1(c), a 6-fold symmetry image (Fig.1(d)) was observed, capturing the boundaries between the non-rotated domain and the rotated domain. The observation point was additionally moved 70 μm, and only the rotated domain was observed (Fig.1(e)). These results corresponded to pole figures. The observation by moving the position in this way revealed the presence of a single domain for the area of 100 μm^2 or larger.

Figure 2(a) shows rocking curves for Ir(111). The full width at half maximum of the rocking curve for Ir(111) deposited by MBE (blue line) was 0.054°. An AFM image is shown in Fig. 2(b). The average roughness height *Ra* was 0.3 nm. The Ir films deposited by sputtering method, we conventionally used, had the FWHM for the rocking curve of 0.139° (red line in Fig.2(a)) and average roughness height *Ra* of 1.3 nm [3]. As a result of the combination of the low-temperature buffer layer, H_2 post-annealing, and the low growth rate in the MBE growth, the Ir(111) thin films deposited by MBE were demonstrated to have high crystallinity and surface flatness.

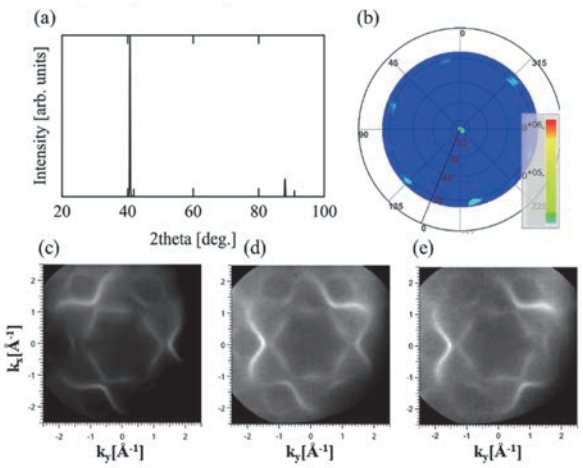

Fig. 1. (a) 2theta/omega profile and (b) pole figure of Ir thin films deposited by MBE. (c)-(e) Iso-energy cross sections of 2D band dispersions of Ir(111) with photon energy of 100 eV. The observation point of (d) was moved 100 μm from (c), and (e) was moved 100 μm from (d).

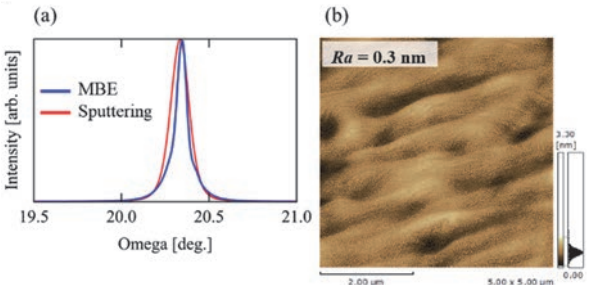

Fig. 2. (a) Rocking curve for Ir(111). Blue line shows deposited by MBE and red line shows deposited by sputtering methods. (b) AFM image of Ir(111) deposited by MBE.

[1] S. Koh *et al*., Appl. Phys. Lett. **109** (2016) 023105.
[2] A. Sakurai *et al*., Jpn. J. Appl. Phys. **59** (2020) SIID01.
[3] E. Hashimoto *et al*., Jpn. J. Appl. Phys. **61** (2022) SD1015.
[4] F. Matsui *et al*., Rev. Sci. Instrum. **94** (2023) 083701.

BL6U, BL7U

Linear Polarization Turntable Measurement of the Band Structure of Au(111)

K. Hagiwara[1], S. Suga[2], S. Tanaka[2] and F. Matsui[1, 3]
[1]*UVSOR Synchrotron Facility, Institute for Molecular Science, Okazaki 444-8585, Japan*
[2]*SANKEN, Osaka University, Mihogaoka 8-1, Ibaraki 567-0047, Japan*
[3]*School of Physical Sciences, The Graduate University for Advanced Studies (SOKENDAI), Okazaki 444-8585, Japan*

Dual-beamline photoelectron momentum microscope (PMM) developed at UVSOR [1] is the first example of the implementation of a dual-beamline combination for PMM apparatus in the world. In 2023, we successfully branched the vacuum ultraviolet (VUV) beamline BL7U and introduced a VUV beam in the normal-incidence configuration in the PMM experimental station [1] in addition to a soft X-ray beam from the beamline BL6U [2, 3]. In particular, normal-incidence PMM is attractive for studying atomic orbitals and spins of the valence electronic states. Highly symmetric photoemission configuration with such normal incidence eliminates the experimental geometry-induced photoemission asymmetry, which necessarily occurred in the grazing-incidence configuration. Thus, normal-incidence PMM enables one to make direct access to atomic orbital information through photon-polarization-dependent transition-matrix-element analysis.

This PMM experimental station allows in-plane sample rotation from azimuthal angle ϕ_s = -90º to 90º, offering detailed measurements with tunable linear polarization geometries. Different experiments with two mutually orthogonal linear polarization geometries can be performed in two ways. 1) switching the photon polarization from vertical to horizontal or 2) rotating the sample by ϕ_s = 90º instead of switching the photon polarization. The former way offers the advantage of keeping the analyzed area always the same. We note that a photon flux of horizontally polarized light is weaker than that of vertical polarized light (one fifth at $h\nu$ = 20 eV) due to the reflectance difference of the branching mirrors at BL7U [1]. Thus, the latter way, *i.e.,* measurements using vertical polarized light with a ϕ_s = 90º difference in azimuthal angle orientation is practical in terms of the efficiency.

In this work, we demonstrate rotational dependence of the linear polarization towards detailed atomic orbital analysis of the valence band structure. A sample of the Au(111) surface was rotated in-plane by ϕ_s and measured using vertically polarized light from the BL7U branch. Here, we show the 2D momentum (k_x, k_y) distribution of photoelectrons with a fixed in-plane sample orientation but rotating the photon polarization vector $\boldsymbol{E}$ in Fig. 1. One can see the features corresponding to the cross section of the Fermi sphere of the bulk gold crystal: the nearly hexagonal contour centered at the $\overline{\Gamma}$ point and the so-called neck features located around the $\overline{M}$ point, which connects the Fermi surfaces of the neighboring Brillouin zones. One can find that photoemission intensities of the nearly hexagonal contour on different momentum points exhibit different modulation with changing rotation angle (ϕ_s) of $\boldsymbol{E}$. This corresponds to the fact that the nearly hexagonal contour on different momentum points is composed of mainly in-plane p orbitals pointing outwards from the $\overline{\Gamma}$ point [4].

[1] K. Hagiwara *et al*., J. Synchrotron Radiat. **31** (2024) 540.
[2] F. Matsui *et al*., Jpn. J. Appl. Phys. **59** (2020) 067001.
[3] F. Matsui *et al*., Rev. Sci. Instrum. **94** (2023) 083701.
[4] F. Matsui *et al*., Phys. Rev. B **72** (2005) 195417.

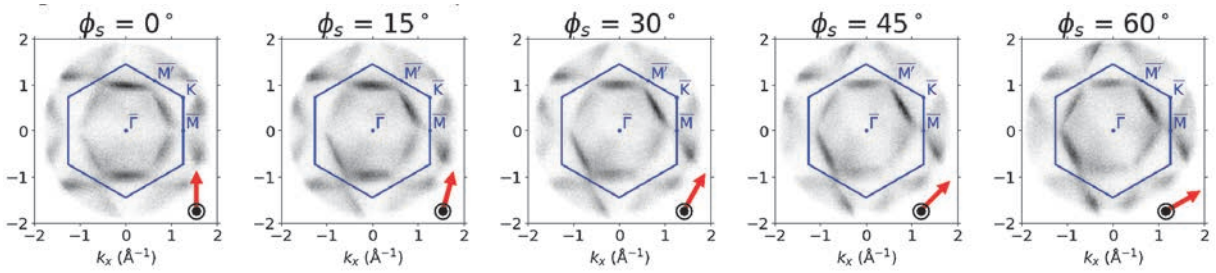

Fig. 1. Turntable measurement of 2D momentum (k_x, k_y) distribution of photoelectrons of the Au(111) surface at $E = E_F$ -1 eV with varied photon polarization vector $\boldsymbol{E}$. The sample was rotated in-plane by ϕ_s and measured using vertically polarized light at $h\nu$ = 20 eV from the BL7U branch. Here, the data were rotated so that the in-plane sample orientation is aligned in the same direction.

ARPES Study of Anomalous Secondary Photoemission from $SrTiO_3$(100)

C.Y. Hong[1,2], P.X. Ran[2,3], X.P. Xie[2,3] and R.-H. He[2]
[1]*Department of Physics, Fudan University, Shanghai 200433, China*
[2]*School of Science, Westlake Institute for Advanced Study, Westlake University, Hangzhou 310064, China*
[3]*Department of Physics, Zhejiang University, Hangzhou 310027, China*

Photocathode materials are crucial components in numerous modern technologies that rely on light detection or electron-beam generation[1-3]. However, most photocathode materials currently used are primarily based on traditional metals and semiconductors. Recently, we reported the observation of spontaneous coherent secondary electron emission (SEE) on the surface of $SrTiO_3$ (STO) after vacuum annealing, with a significantly enhanced peak intensity observed at low temperatures[4]. Spontaneous coherent secondary electron beams can be generated without the need for threshold excitation, even under non-monochromatic light excitation.

The intense coherent photoelectron emission observed on the surface of STO cannot be explained by traditional photoemission theories. To address this challenge, we have recently proposed a new model[5]. Based on the conventional three-step model[6], we introduced an additional step that resembles the Auger effect, establishing a recycling mechanism for failed photoelectrons to analyze this anomalous emission phenomenon in STO. Our model considers the unique energy level structure near the Fermi surface of the valence and conduction bands of STO, enabling high-coherence photoelectron emission under specific photon energy excitations.

To confirm our theoretical model, we needed to excite STO with various photon energies and examine its SEE spectrum. Due to the limitations of our lab-based ARPES setup, which only uses a helium lamp, we conducted systematic ARPES measurements at the BL7U beamline of UVSOR. We investigated the SEE of STO across a range of photon energies (7.1 to 10 eV) and observed a significant dependence on photon energy, as shown in Fig. 1. The positions of Peak 1 and Peak 2 in the SEE spectrum remained constant across varying photon energies, but the intensities of these peaks showed substantial variations.

To further analyze this data, we performed preliminary processing, as depicted in Fig. 2. We found that when the excitation photon energy was below 8.2 eV, there was almost no observable intensity for Peak 1 and Peak 2. However, the peaks began to emerge when the photon energy exceeded 8.2 eV. Notably, for photon energies below 8.8 eV, the intensity of Peak 2 surpassed that of Peak 1, while for energies above 8.8 eV, Peak 1 became the dominant feature. We are currently investigating the relationship between these observations and the band structure more thoroughly.

Additionally, to explore the nonlinearity of SEE intensity, we conducted experiments using white light and different photon energies to investigate the correlation between excitation light intensity and SEE. Finally, we attempted to study the two-dimensional electron gas on the STO surface using low photon energy, but we were unable to obtain meaningful data due to a poor signal-to-noise ratio.

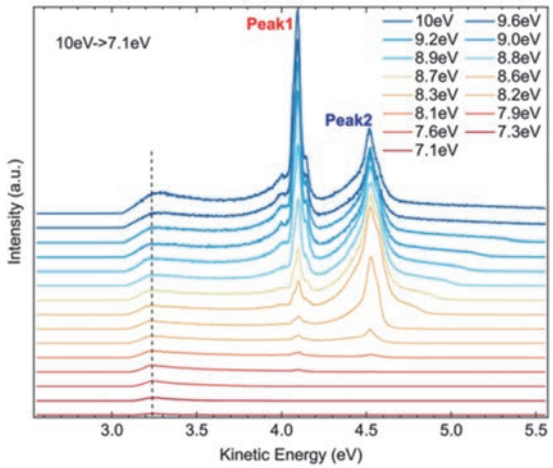

Fig. 1. The secondary electron emission spectra of STO under different photon energies.

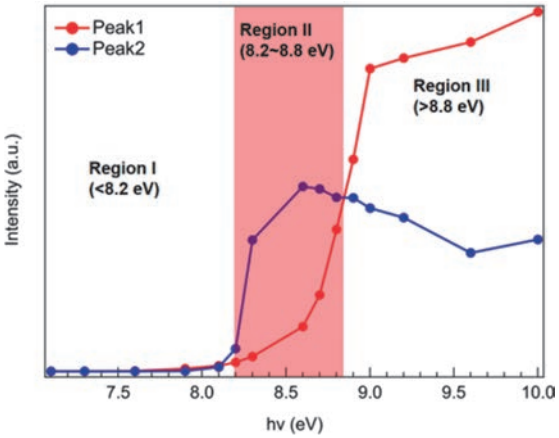

Fig. 2. Peak intensity of the secondary photoemission spectrum versus excitation photon energy.

[1] T. Rao and D.H. Dowell, *An Engineering Guide to Photoinjectors* (CreateSpace, 2013).
[2] G. Sciaini and R.J.D. Miller, Rep. Prog. Phys. **74** (2011) 096101.
[3] P.D. Townsend, Contemp. Phys. **44** (2003) 17.
[4] C. Hong *et al.*, Nature **617** (2023) 493.
[5] M. Matzelle *et al.*, arXiv:2405.06141 (2024).
[6] W.E. Spicer, Phys. Rev. **112** (1958)114.

BL7U

Metal-Insulator Transition in Si(111)√3×√3-Sn

H. Nishimichi[1], K. Ishihara[1], S. Ichinokura[1], K. Tanaka[2] and T. Hirahara[1]
[1]*Deparment of Physics, Tokyo Institute of Technology, Tokyo 152-8551, Japan*
[2]*UVSOR Facility, Okazaki 444-8585, Japan*

High-temperature superconductivity in cuprates has attracted significant interest since its discovery in 1986. However, there is still no consensus regarding its precise mechanism and the complicated relationship between Mott physics, magnetism, and superconductivity. The Si(111)√3×√3-Sn surface, which is formed by 1/3 monolayer (ML) adsorption of Sn onto the Si(111) substrate, has been shown to host similar properties with cuprates and thanks to the simplified atomic structure, it is believed that it may help to unveil the intricate nature of superconductivity doped Mott systems.

Recently, a novel method to induce hole doping in this system was discovered, namely to use a highly p-doped Si substrate [1]. Utilizing this modulation doping, an energy gap was shown to form at low temperature and interpreted as due to the occurrence of superconductivity with d-wave symmetry [2,3]. The superconducting transition temperature reached as high as 9 K, which is much higher than that of typical surface superconductors reported up to now. This calls for a further detailed study to explain the possible high-temperature superconductivity in this system and hopefully apply it to the case of cuprates. Especially up to now, only the local density of states has been measured and information on the detailed macroscopic quantities such as band dispersion and transport properties is still lacking.

Therefore in this study, we measured the electronic structure of the Si(111)√3×√3-Sn surface in detail using samples grown on different substrates. We employed four types of substrates: n-type Si(111) with a resistivity of 0.001-0.0035 Ωcm (n-high), n-type with a resistivity of 1.5-5 Ωcm (n-low), p-type with a resistivity of 5-10 Ωcm (p-low), and p-type with a resistivity of 0.006-0.008 Ωcm (p-high). The Si(111)-7×7 clean surface was prepared by direct current heating up to 1500 K for a few seconds (flashing). Sn was evaporated onto the 7×7 surface at 800 K and then post-annealed for 5 min to form the √3×√3 surface. ARPES was conducted at UVSOR BL-7U with p-polarized photons at hν = 14eV. The energy and angular resolutions were 15 meV and 0.25°, respectively. The Fermi level was determined by measuring a polycrystalline Au film placed near the real sample.

Regardless of the Si substrate used, all the Si(111)√3×√3-Sn samples were found to be metallic at room temperature (RT) and the Fermi surface was the consistent with DFT calculations as shown in Fig. 1. At 7 K, we found that the system becomes insulating as shown in Figs. 2(a) and (b) [red and blue curves]. This is consistent with the fact that the ground state of this surface is a Mott insulator. However, the surface became metallic again by repeatedly annealing the p-high substrate in ultra-high vacuum [green curve in Fig. 2(b)]. The Fermi surface shown in Fig. 2(c) is similar to that measured at room temperature. Thus we have found that not only the substrate type but also the substrate annealing is important in deducing a metal-insulator transition in this surface for the first time. Possible evidence of superconductivity has been obtained for this metallic sample from *in situ* conductivity measurements [4].

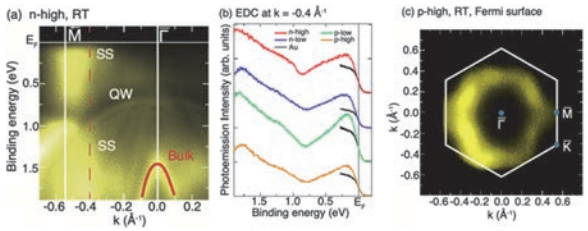

Fig. 1. (a) Band dispersion at room temperature of the Si(111)√3×√3-Sn surface grown on a n-high substrate. (b) Energy dispersion curves (EDC) at k = -0.4 Å^{-1} for Si(111)√3×√3-Sn grown on different Si substrates compared to that for the Au. (c) The Fermi surface (energy contour for a ±20 meV window around the Fermi energy) at room temperature of the Si(111)√3×√3-Sn surface grown on a p-high substrate.

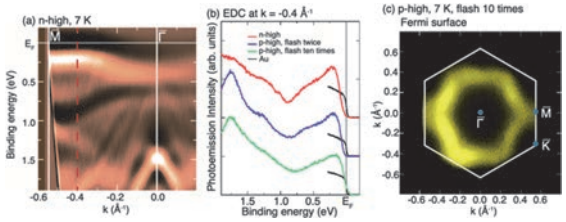

Fig. 2. (a) Band dispersion (second derivative) at 7 K of the Si(111)√3×√3-Sn surface grown on a n-high substrate. (b) EDC at k = -0.4 Å^{-1} for Si(111)√3×√3-Sn grown on different Si substrates compared to that for the Au. (c) The Fermi surface at 7 K of the Si(111)√3×√3-Sn surface grown on a p-high substrate.

[1] F. Ming *et al.,* Phys. Rev. Lett. **119** (2017) 266802.
[2] X. Wu *et al.,* Phys. Rev. Lett. **125** (2020) 117001.
[3] F. Ming *et al.,* Nat. Phys. **19** (2023) 500.
[4] H. Nishimichi *et al*., to be submitted.

Anisotropic Surface Atomic Structure and Electronic State in a YbSb/GaSb(001) Thin Film

Y. Chen[1], T. Nakamura[2,1], S. Sugihara[1], K. Nishihara[1], K. Tanaka[3] and S. Kimura[2,1,4]
[1]*Department of Physics, Graduate School of Science, Osaka University, Toyonaka 560-0043, Japan*
[2]*Graduate School of Frontier Biosciences, Osaka University, Suita 565-0071, Japan*
[3]*UVSOR Synchrotron Facility, Institute for Molecular Science, Okazaki 444-8585, Japan*
[4]*Department of Material Molecular Sciences, Institute for Molecular Science, Okazaki 444-8585, Japan*

Rare-earth mono-pnictides (*REPn*s) are well-known for their various magnetic properties, such as the 'Davil's Staircase' in CeSb, originating from the hybridization of *RE*'s localized 4*f* orbitals and *Pn*'s *p*-orbitals [1,2]. Recently, the emergence of an antiferromagnetic topological insulator phase due to the coupling of the nontrivial topology and the symmetry breaking owing to the antiferromagnetic ordering is reported in NdSb [3]. On the other hand, it has been reported that the breaking of the rotational symmetry of the surface atomic structure can be coupled with nontrivial surface states [4]. Therefore, to explore the potential novel properties in *REPn* with broken rotational symmetry, we are focusing on the epitaxial *REPn* thin film system, where the symmetry of the surface atomic structure could be controlled by surface science methods, such as changing the symmetry of the substrate. In this work, we have fabricated an anisotropic YbSb thin film on GaSb(001) substrates with 2-fold rotational symmetry by the molecular beam epitaxial (MBE) method and studied the electronic state by synchrotron-based angle-resolved photoelectron spectroscopy (ARPES).

The clean Sb-rich GaSb(001)-c(2×6) reconstruction surface was prepared by Ar ion sputtering at 720 K and following evaporation of Sb at the same substrate temperature. After that, Yb and Sb were co-evaporated onto the substrate at 570 K in a 1: 1.1 atomic ratio. Figure 1 shows the LEED pattern of the 14-ML YbSb(001). In addition to integral order diffraction spots of bulk YbSb with NaCl structure observed along the [$\bar{1}$10] direction, the fractional diffraction spots according to the two-fold symmetry are observed in the [110] direction throughout the entire sample surface. This result suggests an anisotropic single-domain (2×1) surface reconstruction.

Figure 2 shows the Fermi surface intensity image measured with horizontally polarized 21-eV photons at a temperature of 7.5 K. A square-like Fermi contour (red dashed line) is observed near the $\bar{\Gamma}$ point, which is consistent well with the Sb 5*p* hole pocket in other reported *RE*Sb systems [5]. On the other hand, the high-intensity area reflecting the Fermi surface extends in the [110] direction, showing a 2-fold rotational symmetry rather than a 4-fold symmetry of the (001) plane in bulk YbSb.

Figure 3 shows the ARPES intensity plots along $\bar{\Gamma}$-$\bar{X}_1$ ([110] direction) and $\bar{\Gamma}$-$\bar{X}_2$ ([$\bar{1}$10] direction) with both horizontally polarized (LH) and vertically polarized (LV) 21-eV photons. Dispersions around $\bar{\Gamma}$ are consistent with each other in both directions. In contrast, new dispersions appear along the $\bar{\Gamma}$-$\bar{X}$ line in the [110] direction, which could be explained by the double period band folding due to the (2×1) surface reconstruction.

The results above suggest that the 4-fold symmetry of bulk YbSb is broken in both the surface atomic structure and electronic state of the fabricated YbSb/GaSb(001) thin film. The lowered surface symmetry will make novel physical properties.

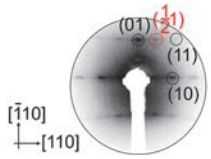

Fig. 1. LEED of the fabricated YbSb thin film measured with 79-eV electrons at 7.5 K.

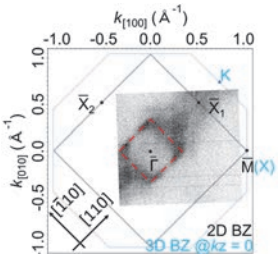

Fig. 2. Fermi surface intensity map measured with horizontally polarized 21-eV photons at 7.5 K.

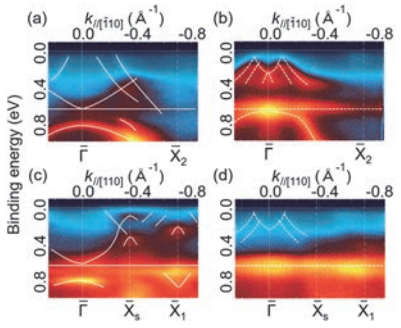

Fig. 3. ARPES intensity plots measured with 21-eV photons at 7.5 K. (a) $\bar{\Gamma}$-$\bar{X}_2$, LH. (b) $\bar{\Gamma}$-$\bar{X}_2$, LV. (c) $\bar{\Gamma}$-$\bar{X}_1$, LH. (d) $\bar{\Gamma}$-$\bar{X}_1$, LV.

[1] J. Rossat-Mignod *et al*., J. Magn. Magn. Mater. **52** (1985) 111.
[2] H. Takahashi and T. Kasuya, J. Phys. C: Solid State Phys. **18** (1985) 2697, 2709, 2721, 2731, 2745, 2755.
[3] A. Honma *et al*., Nat. Commun. **14** (2023) 7396.
[4] Y. Ohtsubo *et al.,* Nat. Commun. **13** (2022) 5600.
[5] H. Oinuma *et al*., Phys. Rev. B: Condens. Matter **96** (2017) 041120(R).

BL7U

Photoelectron Spectra of Thermoelectric Oxide $Ba_{1/3}CoO_2$

S. Tanaka[1], K. Kang[2] and H. Ohta[2]
[1]*SANKEN, Osaka University, Ibaraki 464-0056, Japan*
[2]*Research Institute for Electronic Science, Hokkaido University, Sapporo 001-0020, Japan*

Thermoelectric power conversion technology is one of the key issues for the industry of the future. It converts waste heat into electricity via the Seebeck effect. Its efficiency of the conversion can be estimated by the thermoelectric figure of merit (ZT). In these decays, many efforts have been made to develop thermoelectric materials with high ZT along with the practical advantages, such as low cost, chemical stability, size, flexibility, *etc*. Recently, Ohta's group in Hokkaido University has fabricated a freestanding $Ba_{1/2}CoO_2$ single-crystalline thin film with ZT~0.55 at 600°C in air by the epitaxy method [1], which is very promising for the thermoelectric devices in the near future. Therefore, its detailed electronic structure is highly desired to reveal. In this report, we show results of the photoelectron spectroscopic measurements of the $Ba_{1/2}CoO_2$ film.

The film was prepared by epitaxial method on Al_2O_3 substrate. The crystalline structure of the film was verified by X-ray diffraction and AFM. It was assured that annealing at 300°C in $<10^{-5}$ Pa does not affect the crystalline structure. After the deposition, the sample was exposed to air, transferred to UVSOR, and inserted into the UHV chamber at BL7U. The sample was then heated in UHV ($<10^{-7}$ Pa) to remove the contamination deposited on the sample surface during the transfer.

Figures 1 and 2 show angle-integrated and angle-resolved photoelectron spectra of $Ba_{1/2}CoO_2$ taken at hν=36eV at room temperature. Before the measurements, the sample was heated at 200, 250 and 350 °C. for 30 min, respectively. The sample surface heated at 350C apparently showed the change of colors at depending on the position of the sample, and spectra were taken at typical two positions (A, and B). The sample color is more changed at the position B than the position A. One thing that should be pointed out is a fact there is no density of states to cross the Fermi level for all the spectra. Considering the high surface sensitivity of the photoelectron spectroscopy, it indicates that the sample surface is not metallic. It is surprising since the bulk resistivity of the sample is 0.001Ωcm. Therefore, the sociometric condition of the sample surface seems not same as the inside the film. The angle-integrated spectra gradual changes as functions of the heating temperatures. As the heating temperature is higher, the intensity of the peak nearest to the Fermi level, which mainly consists of the Co3d orbital, becomes smaller in intensity. One more characteristic change in the spectra is that decrease of the peak around -15eV. This peak can be assigned as the Ba5p semicore level. The depression of this peak at the position B after the 350°C may indicate the evaporation of Ba near the surface layer atom starts at 350°C, although the bulk data showed that it is stable upto 600°C. The angle-resolved spectra show that there is no dispersion observed. Therefore, the surface is not well crystalized at any heating temperature, and the heating in vacuum cannot produce a well-defined surface. For studying ARPES of the $Ba_{1/2}CoO_2$ more, the other method, e.g., in-situ epitaxial growth, is required.

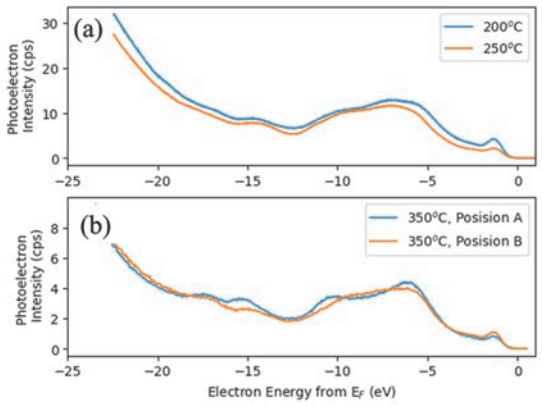

Fig. 1. Angle-integrated photoelectron spectra of $Ba_{1/2}CoO_2$ epitaxially produced on Al_2O_3 substrate and heated at 200°C and 250°C for 30 min (a), and those taken at different positions of the sample heated at 350°C for 30 min (b).

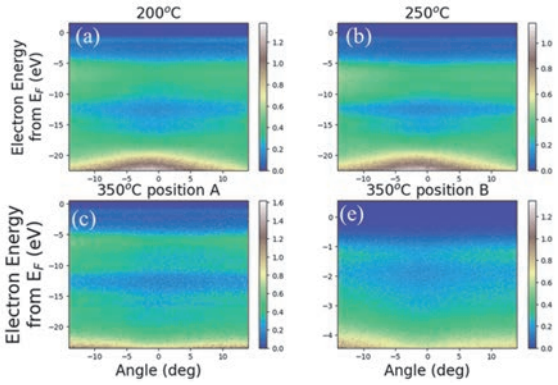

Fig. 2. Angle-resolved photoelectron spectra of $Ba_{1/2}CoO_2$.

[1] K. Kang *et al*., ACS Appl. Electron. Mater. **5** (2023) 5749.

BL7B

Electronic States at Ionic Liquid/Electrode Interfaces by Multi-Angle Incidenct-Angle ATR-UV-Vis Spectroscopy

I. Tanabe[1], T. Kakinoki[2] and K. Fukui[2]

[1]*Department of Chemistry, College of Science, Rikkyo University, Toshima 171-0021, Japan*

[2]*Department of Materials Engineering Science, Graduate School of Engineering Science, Osaka University, Toyonaka 560-8531, Japan*

Ionic liquids are salts in the liquid phase at room temperature and atmospheric pressure which have recently attracted much attention in various fields such as electrochemistry and synthetic chemistry. In particular, due to unique features such as extremely low vapor pressure, high thermal stability, and wide potential window, ionic liquids are promising as novel electrolytes that are both safe and functional. In electrochemical devices the electrolyte/electrode interface is essentially important. Recently, we reported electronic transition spectra in the 140−450 nm region of various ionic liquids by using the attenuated total reflectance (ATR) technique. Additionally, a new spectroscopic system, namely electrochemical-ATR (EC-ATR) ultraviolet-visible spectroscopy, which can access the interfacial area, was developoed [1, 2].

In this study, we measured ATR spectra in ionic liquid/gold electrode interface using polarized UV lights from BL7B at the UVSOR. We deposited the gold thin film on the sapphire ATR prism using physical vapor deposition method and used it as the working electrode. As the electrolyte, we adopted EMIM-TFSI (1-Ethyl-3-methylimidazolium bis(trifluoromethanesulfonyl)imide). Platinum mesh and platinum rod are utilized as the pseudo counter electrode and reference electrode, respectively. We applied the negative potentials to the gold electrode using cyclic voltammetry from 0 V to −1.8 V vs. Pt, and measured the ATR absorbance spectra simultaneously.

Figure 1 depicts the difference ATR spectra induced by the negative electrode potential. The incident light comprised (a) non-polarized light from a deuterium lamp and (b) s-polarized light from BL7B at UVSOR, respectively. In both spectra, the ATR absorbance wavelength shifted with the applied potentials. Due to the negative electrode potential applied to the electrode, EMIM cations approached the gold electrode surface, while TFSI anions were electrostatically repelled from the electrode surface. The spectral changes may reflect such phenomena near the electrode surface. Furthermore, polarized probe light can distinguish the orientation of the interfacial species in the ATR spectra: s-polarized light resonates with the dipole moment whose direction is parallel to the interface, while p-polarized light resonates with the perpendicular component. It is known that the imidazolium cation orients its structure on the negatively charged electrode, with the imidazolium rings becoming parallel to the interface [3]. Thus, we can assume that the difference spectra are mainly attributed to the parallel orientation of the imidazolium cation ring in the first layer of the interface. In summary, we suggest the possibility of utilizing the polarization of the probe light in ATR spectroscopy.

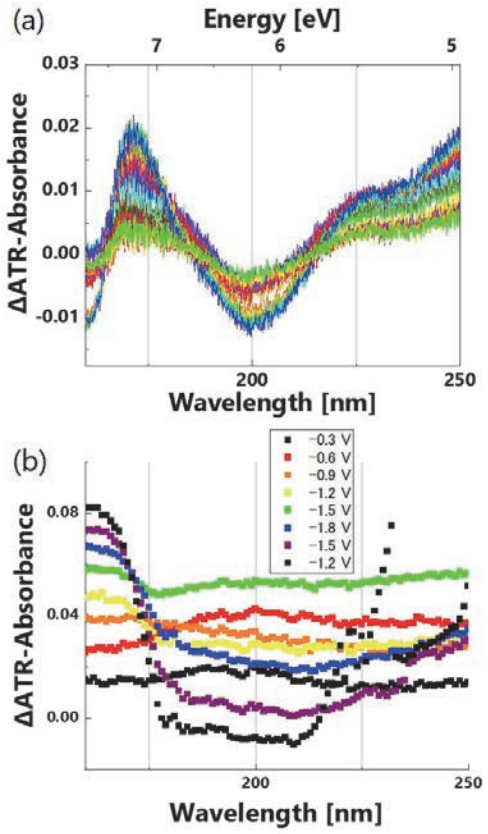

Fig. 1. Difference ATR-UV spectra induced by the negative electrode potential using (a) non-polarized light and (b) s-polarized light.

[1] I. Tanabe *et al*., Anal. Chem. **91** (2019) 3436.
[2] I. Tanabe *et al*., Commun. Chem. **4** (2021) 88.
[3] H. Miyamoto *et al*., Phys. Chem. Chem. Phys. **20** (2018) 19408.

III-4

UVSOR User 6

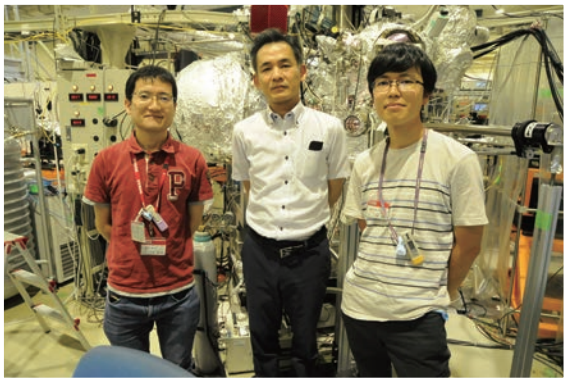

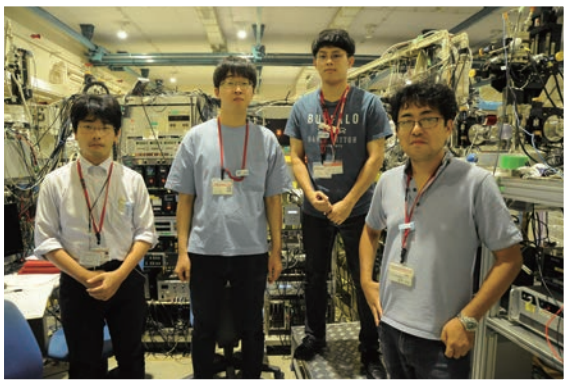

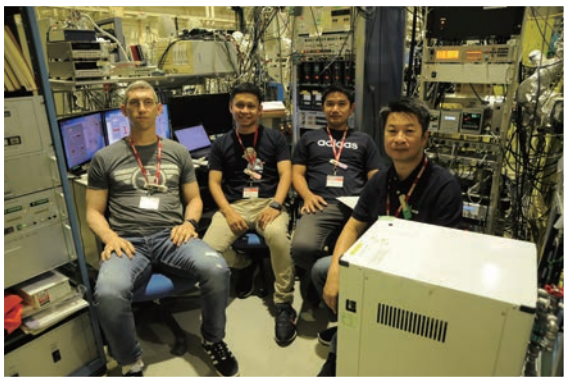

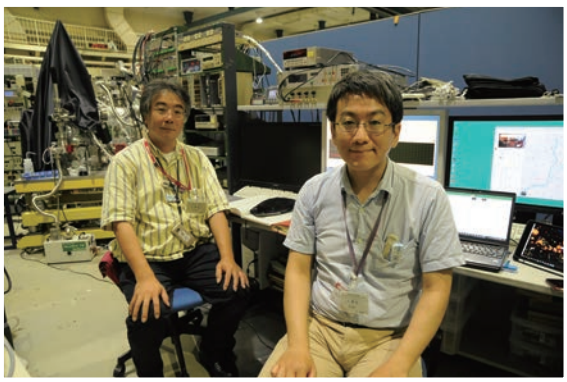

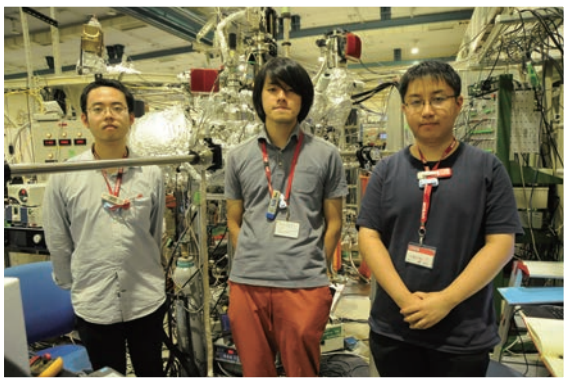

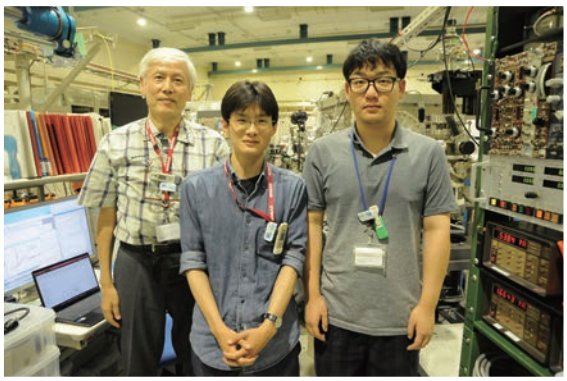

UVSOR User 7